ON THE APPLICATION OF PMU MEASUREMENTS TO SYSTEM STABILITY ANALYSIS

BY

JIANGMENG ZHANG

THESIS

Submitted in partial fulfillment of the requirements
for the degree of Master of Science in Electrical and Computer Engineering
in the Graduate College of the
University of Illinois at Urbana-Champaign, 2012

Urbana, Illinois

Adviser:

Assistant Professor Alejandro D. Domínguez-García

ABSTRACT

This thesis proposes a method to analyze power system stability by utilizing PMU measurements. As the current power system is operated close to its limits, stability is of high concern for both operators and customers. The implementation of phasor measurement units across the power system allows for accurate and fast stability monitoring and analysis. To address the application of PMU measurements to stability monitoring, we propose the use of circuit equivalent ideas for both voltage and angle stability. This method is applicable for on-line steady-state stability assessment, without knowing the system topology. For voltage stability, parameter estimation methods are investigated to address the tradeoff between accuracy and computational speed. For angle stability, a modified model is presented to reflect the fact that the main change of the system occurs inside the equivalent system. Next, by taking advantage of PMU high measuring frequency, which provides a high resolution to monitor the systems, a frequency domain analysis based method is proposed to estimate the system equivalent inertia, which enables further dynamic stability analysis. The methods are illustrated with several simulated and real case studies. These algorithms are identified as effective and simple methods to analyze system stability.

To my parents and brother, for their love and support.

ACKNOWLEDGMENTS

I have been deeply grateful to my adviser, Professor Alejandro D. Domínguez-García, over the past two years; his passion and patience, as well as his bright vision, have been invaluable to me. Without his guidance and support, this work would not have been possible. I would also like to thank Professor Peter W. Sauer for all of the advice throughout this project, from which I have enjoyed the beauty of simplicity in science. Many thanks also go to Joyce Mast, for her editorial help on this thesis. Finally, I would like to thank my family and friends for their continued support.

CONTENTS

LIST OF TABLES

LIST OF FIGURES

LIST OF ABBREVIATIONS

AAS	Angle Across System
DF	Dominant Frequency
DFT	Discrete Fourier Transform
FFT	Fast Fourier Transform
LSE	Least Squares Estimation
LSEMW	Least Squares Estimation with Moving Window
PDC	Phasor Data Concentrator
PMU	Phasor Measurement Unit
RLSE	Recursive Least Squares Estimation with Fading Factor
RTDS	Real Time Digital Simulator
SM	Stability Margin
TE	Thévenin Equivalent

LIST OF SYMBOLS

$\bar{E}$	Thévenin-equivalent (TE) voltage source. $\bar{E} = E\angle\delta = E_r + jE_i$.
E	Magnitude of $\bar{E}$
δ	Angle of $\bar{E}$
E_r	Real part of $\bar{E}$
E_i	Imaginary part of $\bar{E}$
$\bar{Z}_{th}$	Thévenin-equivalent (TE) impedance. $\bar{Z}_{th} = R_{th} + jX_{th}$.
R_{th}	Real part of $\bar{Z}_{th}$
X_{th}	Imaginary part of $\bar{Z}_{th}$
H	Inertia

Chapter 1

INTRODUCTION

As the current power system is operated close to its limits, stability is of high concern for both operators and customers. Stability is the ability of a power system to maintain an acceptable state after being subjected to a disturbance. Generally power system stability can be classified into two categories: angle stability and voltage stability [1]. Angle stability is the ability of interconnected synchronous machines to stay in synchronism. Voltage stability is the ability of a power system to maintain acceptable voltages, particularly for load buses. Stability analysis aims to identify the system stability margin under normal operation and predict the system performance if a disturbance occurs. Both angle stability and voltage stability analyses typically include steady-state analysis, which is concerned with system loadability, and dynamic stability analysis, which deals with system response to disturbances. A diagram showing the classification of power system stability is given in Fig. 1.1.

The implementation of phasor measurement units (PMU) across the power system allows for accurate and fast stability monitoring and analysis. The advantages of PMU measurements over traditional power system supervisory control and data acquisition (SCADA) measurements include: *i*) higher sam-

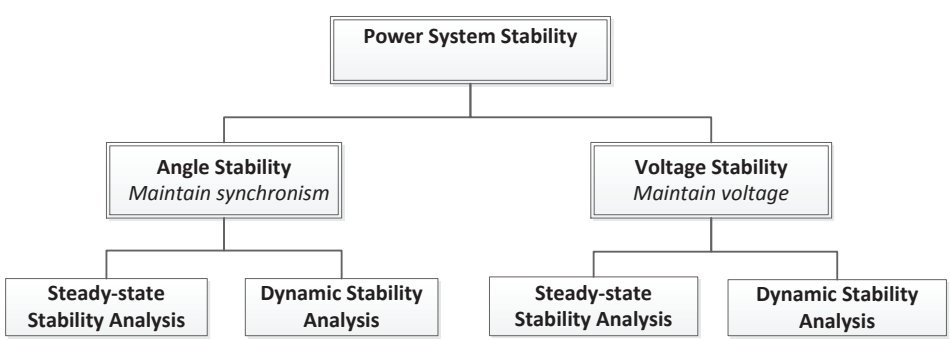

Figure 1.1: Power system stability classification [1].

pling frequency, and *ii*) the ability to provide direct measurement of power system states (i.e., the voltage magnitude and phase angle of each bus) [2]. The high sampling frequency enables PMUs to capture system changes at a much smaller time scale, allowing for more accurate analysis of power systems and faster remedial actions. As to the state measurement, while traditional SCADA system estimates the system states based on voltage magnitudes and power values, PMUs, by making use of the synchronized time signals from Global Positioning System (GPS) system, provide direct measurement of the system states, which can be directly used to analyze system stability.

Various approaches to address the application of PMU data have been explored in the context of power system stability assessment. These approaches include signal processing methods and system equivalent estimation methods. Three signal processing algorithms, namely Prony, Matrix Pencil and Hankel Total Least Squares methods, have been applied to power system analysis [3]. The performance of Prony method on power system stability assessment is explored in [4]. Matrix Pencil method and Hankel Total Least Squares method are adopted to address the computational efficiency and noise issues [5]. Signal processing based methods aim to capture valuable detailed information from the measurements, which is intended to reflect the system operating conditions. There are no physical models involved in these methods. As a result, the methods perform well for transient stability analysis. But they are generally computationally intensive and cannot reflect the wide area system steady stability conditions. System equivalent based methods have been explored to address these issues. For example, the authors in [6] proposed the idea of using Thévenin equivalents to analyze voltage stability. The authors in [7] extend this idea further and presents a voltage instability index based on computing of Thévenin equivalents using PMU measurements. The Thévenin equivalent parameter estimation becomes complicated when it comes to angle stability analysis, because the assumption made in voltage stability analysis that Thévenin equivalent parameters keep constant does not hold. To address this issue, a measurement-based framework using a dynamic equivalent model is proposed in [8, 9] to estimate the equivalent parameters.

Applying equivalent techniques to stability analysis in terms of both load bus voltage stability and transmission system angle stability is challenging. In this thesis, we begin by investigating voltage stability monitoring meth-

ods based on PMU measurements. The Thévenin equivalent based method for voltage stability analysis is implemented on a benchmark system and the noise issue of PMU measurements is addressed by developing modified recursive least squares estimation methods. Next, an equivalent circuit model for transmission systems is proposed to assess the system angle stability. The corresponding parameter estimation method is described as well. For this methodology, the simplicity of the equivalent system and topology-less property result in good computational efficiency and allow for real-time online applications. In addition, besides the stability assessment in terms of steady state as discussed above, we also present a method to estimate the system equivalent inertia by making use of the PMU measurements frequency domain information. Therefore, the dynamic model with estimated parameters also makes possible dynamic stability analyses (e.g., fault clearing time analysis). This set of proposed methods has been validated through simulations in a real time digital simulator (RTDS)/PMU/Phasor Data Concentrator (PDC) testbed. This methodology is also applied to analyze PMU measurements obtained from a real power grid.

This thesis is organized as follows. Related background information, including stability analysis, PMU measurements and Thévenin equivalent, is introduced in Chapter 2. In Chapter 3, we investigate the performance of voltage stability assessment method based on Thévenin equivalents. Least squares estimation methods are developed to address the noise issue from PMU measurements. We extend the equivalent idea to transmission systems stability assessment in Chapter 4 and propose a parameter estimation method based on classical models. Chapter 5 further explores the ideas in Chapter 4 to estimate the system inertia. A real time simulation testbed is introduced as well to perform the experiment in Chapter 5. Next, we apply the method proposed in previous chapters to a real power system PMU data in Chapter 6. Finally, concluding remarks and future work are presented in Chapter 7.

Chapter 2

BACKGROUND

In this chapter, background knowledge is introduced to provide the foundation for further discussion of the work presented in this thesis. The concepts and criteria for power system stability are first described. Synchronized phasor measurements, as a new measurement technique of choice for electric power systems, are introduced. Thévenin equivalent technique, by which the work in this thesis is motivated, is described in Section 2.3.

2.1 Power System Stability

2.1.1 Voltage Stability

Voltage stability is the ability of a power system to remain at acceptable voltages, particularly of load buses. A criterion for voltage stability is that the bus voltage magnitude increases along with the reactive power injection at the same bus. In other words, if the bus voltage magnitude decreases when the reactive power injection at the same bus is increased, the system is unstable in terms of voltage stability [1].

As an example, a simple radial system, consisting of one generator and one load, is illustrated in Fig. 2.1. The impedances of transmission line and load are denoted by $\bar{Z}_{ln}$ and $\bar{Z}_{ld}$ respectively. The active power transferred to the load can be increased by decreasing the load impedance. If we keep decreasing the load impedance, the active power transferred reaches maximum when the magnitudes of $\bar{Z}_{ln}$ and $\bar{Z}_{ld}$ are equal (i.e., $Z_{ln} = Z_{ld}$). After this point, the continuous decrease in load impedance will reduce the transferred power rather than increase it. If the load is with constant-power characteristics, the system becomes unstable [1]; the proof for this stability criterion can be found in Appendix A. Therefore, for this system, the equality of Z_{ln} and Z_{ld}

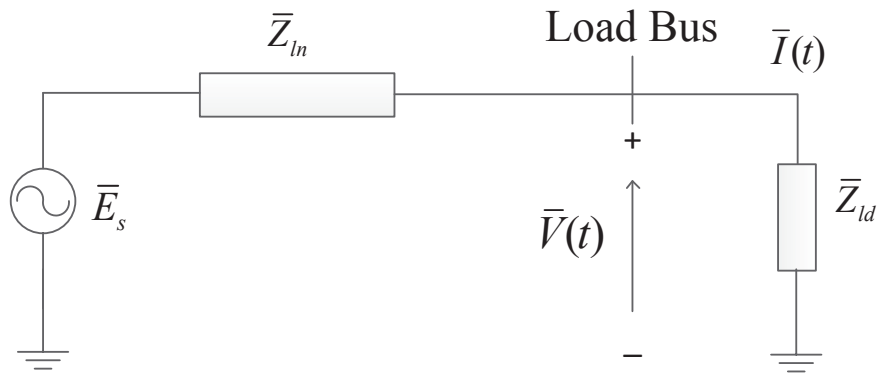

Figure 2.1: Voltage stability illustration.

is a criterion for the voltage stability analysis.

2.1.2 Angle Stability

Angle stability is the ability of interconnected synchronous machines to stay in synchronism. An important characteristic that has a bearing on angle stability is the relationship between interchange active power and angle difference among the synchronous machines [1].

As an example, a simple system comprised of two machines and one transmission line is illustrated in Fig. 2.2. The active power transferred across this system is given by

$$P = \frac{E_1 E_2}{X_1 + X_{ln} + X_2} \sin(\delta_1 - \delta_2), \tag{2.1}$$

from which we can see that, when $\delta_1 - \delta_2$ is zero, P is zero. As the angle difference is increased, the power transferred increases until the angle

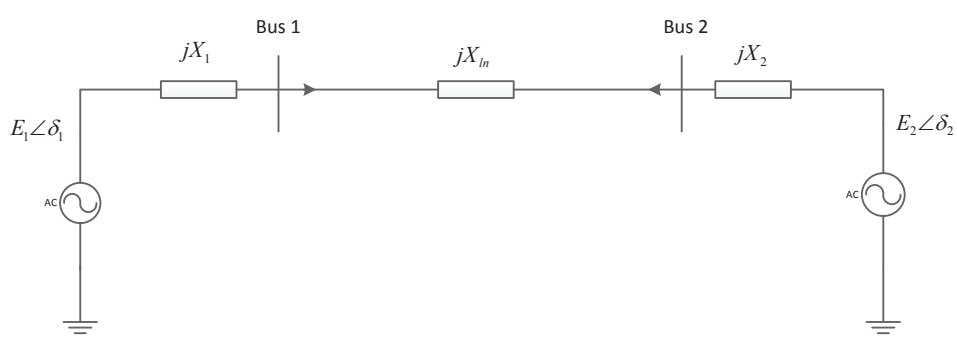

Figure 2.2: Angle stability illustration.

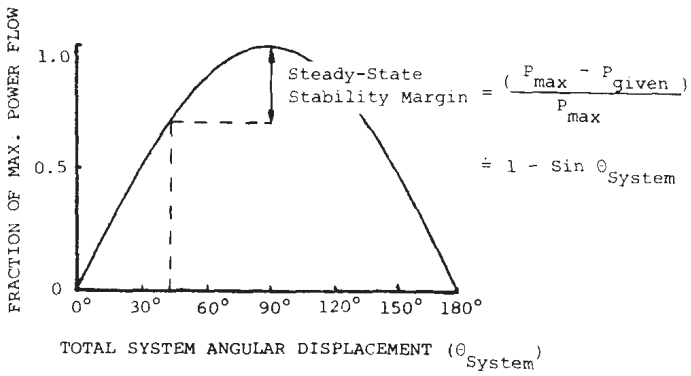

Figure 2.3: Relationship between power and angle difference [10].

difference reaches 90 degrees. After that, a further increase in the angle difference reduces the power transferred in the system. Thus, there is a maximum steady-state power that this system can transfer, which corresponds to 90-degree angle difference [1]. The stability of this power system can be measured by a function of the angle difference, which is called stability margin (SM) given by

$$SM = \frac{P_{max} - P}{P_{max}} = 1 - \sin(\delta_1 - \delta_2). \tag{2.2}$$

The relationship between the power transferred and the angle difference and the concept of stability margin are well illustrated in Fig. 2.3 from [10].

2.2 Phasor Measurement Unit (PMU)

Phasor measurement units (PMUs) are able to measure the phase angle of voltages and currents across the power grid by making the use of the synchronized time signal from the Global Positioning System (GPS). In this way, the power system states can be directly measured out rather than estimated by the traditional SCADA system. In addition, PMUs can sample the voltage and current signals synchronously with 1 microsecond accurary using GPS, while SCADA system estimates the states with 1 second accuracy at most. In the early 1980s, the first prototypes of PMUs using GPS were built at the Power Systems Research Laboratory at Virginia Tech [2]. Currently, the U.S. has installed more than 287 networked PMU and at least 800 PMUs are expected to be installed under smart grid investment grant program by 2013 [11]. With the development of PMUs, research on applications of the

measurements they provide becomes necessary. The basic concepts used in PMU to obtain phasor measurements are presented here.

2.2.1 Phasor Representation

The full description of a phasor representation can be found in [2]. The main ideas are summarized here. Consider a sinusoidal signal (e.g., voltage and current) given by

$$x(t) = \sqrt{2}X\cos(\omega t + \phi) = \sqrt{2}X\cos(2\pi f t + \phi), \tag{2.3}$$

where X is the root mean square (RMS) value of this signal. The signal can be written as

$$x(t) = \Re\{\sqrt{2}Xe^{j(\omega t+\phi)}\} = \Re\{e^{j\omega t}\sqrt{2}Xe^{j\phi}\}. \tag{2.4}$$

It is customary to suppress the term $e^{j(\omega t)}$ since the system frequency ω or f is constant in steady state. Therefore, the sinusoidal signal can be represented by a complex number $\bar{X}$ known as the *phasor*:

$$x(t) \leftrightarrow \bar{X} = Xe^{j\phi}. \tag{2.5}$$

The sinusoidal signal and its phasor representation are illustrated in Fig.2.4. The phasor representation of a sinusoidal signal can be obtained using discrete Fourier transform on samples of the singal.

2.2.2 Phasor Measurements

In PMUs, the computation of phasors of voltages and currents begins with samples of the waveform $x(t)$. Let the sampling frequency be N times the signal frequency (i.e., Nf). Then the uniform interval between two samples ΔT is equal to $\frac{1}{Nf}$. The sampled discrete signal $x_d(n)$ is obtained as

$$x_d(n) = x(n\Delta T). \tag{2.6}$$

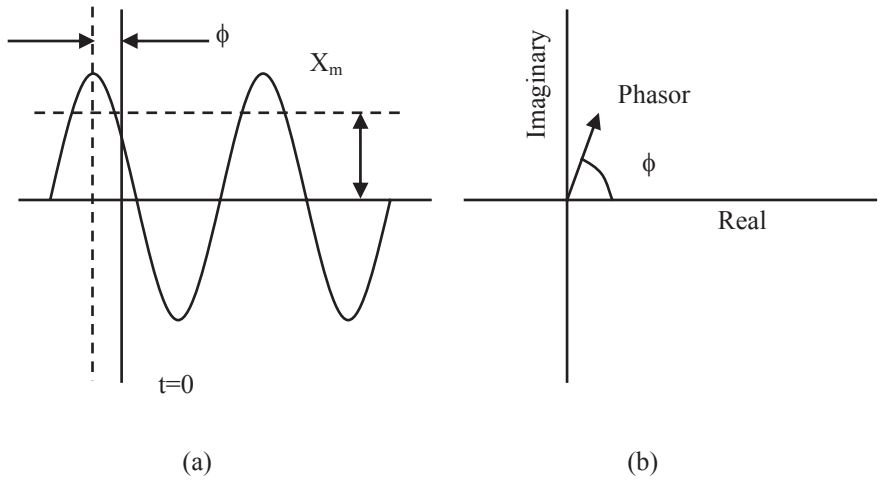

Figure 2.4: A sinusoidal signal and its phasor representation [2].

Using the discrete Fourier transform (DFT), the frequency domain of the discrete signal $x_d(n)$ can be expressed as:

$$\bar{X}_D(k) = \frac{\sqrt{2}}{N} \sum_{n=0}^{N-1} x_d(n) e^{-j(2\pi/N)kn}, \quad 0 \leq k \leq N-1, \tag{2.7}$$

and the phasor representation of the kth harmonic component is given by the magnitude and phase angle of $\bar{X}_D(k)$.

Since the main interest in phasor measurements is the fundamental frequency f component, k is set to be 1. Therefore, the phasor representation of the signal is calculated by

$$\bar{X} = \bar{X}_D(1) = \frac{\sqrt{2}}{N} \sum_{n=0}^{N-1} x_d(n) e^{-j(2\pi/N)n}. \tag{2.8}$$

2.2.2.1 Phasor Measurements of Off-Nominal Frequency Signals

A practical issue about phasor measurements is that phasors are a steady-state concept in terms of frequency; but a power system is never in steady state. The frequency of voltage and current fluctuates around nominal frequency due to the variation of the loads and generations. Since PMU still samples at frequcy of N times norminal frequency, there is some inaccurary in the phasor representation. As in practical power systems, the deviation

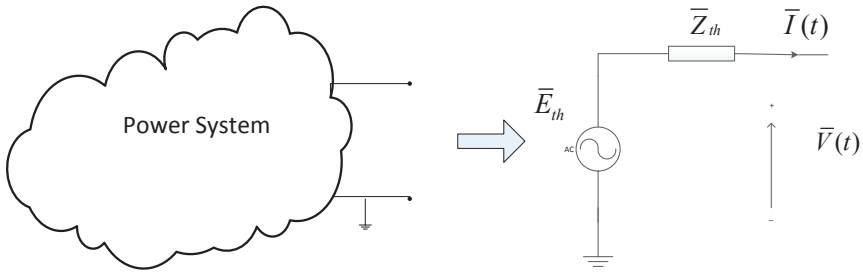

Figure 2.5: Thévenin equivalent.

of system frequency ω from the nominal frequency ω_0 is very small. Then the phasor is approximately rotating counterclockwise at an angular speed of $\omega - \omega_0$ [2]. It is essential to keep this feature in mind when using PMU measurements.

2.3 Thévenin Equivalent (TE)

In circuit theory, the Thévenin theorem states that any DC linear electrical network with two terminals can be equivalent to a combination of a single voltage source and a resistor in series. It is a simplification technique widely used in electric system analysis. For single frequency AC systems, Thévenin theorem holds in the sense that the equivalent is a combination of a AC voltage source and an impedance in series. For power systems, the frequency is maintained to a fixed value (60 Hz for the U.S. power grid). In addition, even though there might be some components with nolinear characteristics involved, for a short analysis period, it is appropriate to linearize the models to satisfy the conditions of the Thévenin theorem. Therefore, it is appropriate to represent the equivalent a power system with two terminals by a combination of an equivalent voltage source and an equivalent impedance, as illustrated in Fig. 2.5.

Chapter 3

VOLTAGE STABILITY

3.1 Introduction

Voltage stability assessment based on Thévenin equivalent (TE) is one of the most common applications of phasor measurements (i.e., PMU data).

For a power system, as shown in Fig. 3.1a, one PMU is set up on the load bus to measure and record the voltage and current phasors. From the perspective of the load bus, the system can be equivalenced to the system in Fig. 3.1 according to Thévenin's theorem. Based on the PMU measurements, it is possible to estimate the TE parameters [12, 13]. With this equivalent system, the system performance situation can be indicated by the distance of Z_{ld} and Z_{th}.

In this framework, the key point is to estimate the TE parameters. Compared to the relatively fast and large load change, we are able to assume that the TE is constant during a short period in order to perform the standard procedure to estimate the TE parameters. However, we have to acknowledge that the whole power system changes all the time and TE parameters are variables in terms of a long time period. The challenge is to keep tracking the TE parameters. To capture the latest TE, only the latest two pairs of measurements need to be used. However, to reduce the impact of noise, many more pairs of measurements during a longer period are needed. To address this issue, moving window and fading factor are incorporated in least squares estimations (LSE) [14].

In this chapter, the voltage stability assessment method is illustrated in Section 3.2. Advanced data processing techniques deriving from LSE method are developed to address the parameter-tracking challenge in Section 3.3. Finally, case studies are performed to validate this stability assessment method and demonstrate the improvement of the modified estimation method in Sec-

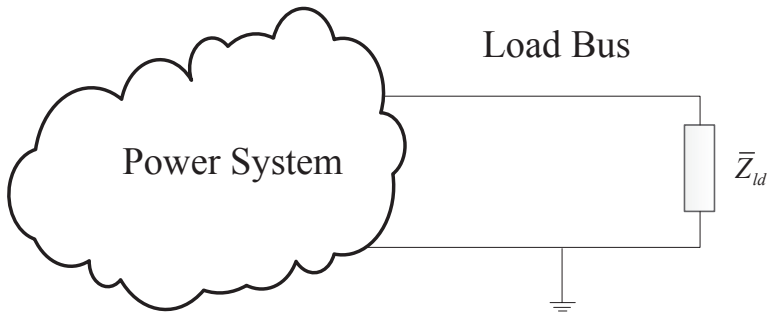

(a) A power system.

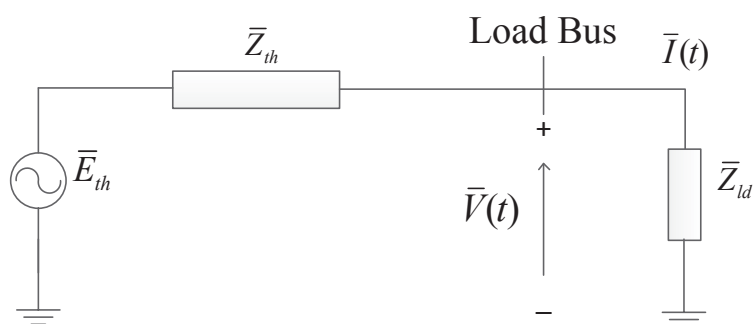

(b) Thévenin equivalent.

Figure 3.1: Thévenin equivalent at load bus.

tion 3.4.

3.2 Voltage Stability Assessment Method

3.2.1 Thévenin Equivalent Parameter Estimation

The authors in [6, 15] proposed that the Thévenin equivalent parameters ($\bar{E}$, $\bar{Z}_{th}$) can be obtained based on Kirchhoff's voltage law with PMU measurements through the following equation:

$$\bar{E} - \bar{I} \cdot \bar{Z}_{th} = \bar{V}, \tag{3.1}$$

where $\bar{V}$ is the voltage phasor at the terminal bus and $\bar{I}$ is the current phasor following into the load.

Consider the system in Fig. 3.1. Let $\bar{E} = E\angle\delta = E_r + jE_i, \bar{Z}_{th} = R_{th} + jX_{th}, \bar{V} = V\angle\theta = V_r + jV_i$ and $\bar{I} = I\angle\gamma = I_r + jV_i$. The complex equation

(3.1) can be rewritten as two real-valued equations with four unknown real parameters (i.e., E_r, E_i and R_{th}, X_{th}) as follows:

$$\begin{bmatrix} 1 & 0 & -I_r(t) & I_i(t) \\ 0 & 1 & -I_i(t) & -I_r(t) \end{bmatrix} \times \begin{bmatrix} E_r \\ E_i \\ R_{th} \\ X_{th} \end{bmatrix} = \begin{bmatrix} V_r(t) \\ V_i(t) \end{bmatrix}. \tag{3.2}$$

Assume that, during a short period, the Thévenin equivalent parameters stay relatively constant. At least 2 pairs of measurements obtained at time t_1 and t_2, during the short period, are required to form 4 equations as shown in the following to estimate the 4 parameters.

$$\begin{bmatrix} 1 & 0 & -I_r(t_1) & I_i(t_1) \\ 0 & 1 & -I_i(t_1) & -I_r(t_1) \\ 1 & 0 & -I_r(t_2) & I_i(t_2) \\ 0 & 1 & -I_i(t_2) & -I_r(t_2) \end{bmatrix} \times \begin{bmatrix} E_r \\ E_i \\ R_{th} \\ X_{th} \end{bmatrix} = \begin{bmatrix} V_r(t_1) \\ V_i(t_1) \\ V_r(t_2) \\ V_i(t_2) \end{bmatrix}, \tag{3.3}$$

3.2.1.1 Applying Incremental Vector

Since one of our goals is to track the system situation online, the speed of algorithm is a main factor to investigate. There are two points that can help us simplify the calculations:

- Instead of real values, complex number equations (i.e., (3.1)) can be directly used in the parameter estimation process. The equation with two pairs of measurements can be simplified as

$$\bar{V}(t_1) = \bar{E} - \bar{I}(t_1)\bar{Z}_{th} \tag{3.4a}$$
$$\bar{V}(t_2) = \bar{E} - \bar{I}(t_2)\bar{Z}_{th}, \tag{3.4b}$$

  which can be expressed in matrix form:

$$\begin{bmatrix} \bar{V}(t_1) \\ \bar{V}(t_2) \end{bmatrix} = \begin{bmatrix} 1 & -\bar{I}(t_1) \\ 1 & -\bar{I}(t_2) \end{bmatrix} \times \begin{bmatrix} \bar{E} \\ \bar{Z}_{th} \end{bmatrix}. \tag{3.5}$$

- For voltage stability, only the Thévenin impedance is of our interest. In (3.4), by subtracting the equation (3.4a) from (3.4b), we can obtain one

equation with only Thévenin impedance and incremental measurements $\Delta\bar{V} = \bar{V}(t_2) - \bar{V}(t_1)$ and $\Delta\bar{I} = \bar{I}(t_2) - \bar{I}(t_1)$:

$$\Delta\bar{V} = -\Delta\bar{I}\bar{Z}_{th}, \tag{3.6}$$

which can further simplify the computation process.

3.2.2 Voltage Stability Assessment

Using the Thévenin equivalent system, the voltage stability can be readily measured based on the fact that maximum power transfer is reached, or in the other words, voltage instability occurs when the magnitude load impedance is equal to that of the TE impedance (i.e., $Z_{ld} = Z_{th}$). Therefore, assessing the closeness to voltage instability, which we refer to as stability margin (SM), can be achieved by measuring the distance of Z_{ld} to Z_{th}:

$$SM = |\frac{Z_{ld} - Z_{th}}{Z_{ld}}|.$$

When $Z_{ld} \gg Z_{th}$, SM is close to 100%, which indicate this system can securely supply the load. When $Z_{ld} \approx Z_{th}$, SM is close to 0%, which means the system is operating around the limit.

3.3 Data Processing Techniques

In realty, noise in the measurements is unavoidable. In order to reduce the impact of noise and estimate the parameters more accurately, more than two pairs of measurements are required in the parameter estimation processing. However, on the other hand, the Thévenin equivalent of the power grid is not strictly constant because it is still a dynamic system, just with a relatively large time constant. Therefore, the time period of the measurements used for parameter estimation cannot be too long; otherwise, the state of the system will change so much that the assumption about constant parameters can no longer hold.

To address this tradeoff, two state estimation methods are introduced. A third method, combining the features of the previous two methods, is also proposed for the specific characteristics of the systems of interest here.

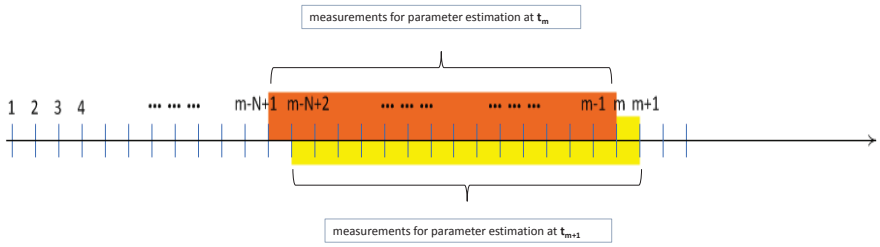

Figure 3.2: Power system stability assessment approaches.

3.3.1 Least Squares Estimation with Moving Window (LSEMW)

As shown in Fig. 3.2, only the latest N pairs of measurements are utilized to estimate the parameters. Let

$$\bar{Y}(t_k) = \bar{H}(t_k)\bar{X}(t_k) \tag{3.7}$$

represent the equation obtained from measurements at time t_k, where

$$\bar{Y}(t_k) = \begin{bmatrix} V_r(t_k) \\ V_i(t_k) \end{bmatrix};$$
$$\bar{H}(t_k) = \begin{bmatrix} 1 & 0 & -I_r(t_k) & I_i(t_k) \\ 0 & 1 & -I_i(t_k) & -I_r(t_k) \end{bmatrix};$$
$$\bar{X} = \begin{bmatrix} E_r \\ E_i \\ R_{th} \\ X_{th} \end{bmatrix};$$

or in vector form,

$$\bar{Y}(t_k) = \bar{V}(t_k);$$
$$\bar{H}(t_k) = \begin{bmatrix} 1 & -\bar{I}(t_k) \end{bmatrix};$$
$$\bar{X} = \begin{bmatrix} \bar{E} \\ \bar{Z}_{th} \end{bmatrix}.$$

Therefore, to estimate the TE parameters at time t_M, the measurements from time t_{M-N+1} to t_{t_M} are utilized and the equation forms as follows:

$$\underbrace{\begin{bmatrix} \bar{Y}(t_{M-N+1}) \\ \bar{Y}(t_{M-N+2}) \\ \vdots \\ \bar{Y}(t_M) \end{bmatrix}}_{\bar{Y}} = \underbrace{\begin{bmatrix} \bar{H}(t_{M-N+1}) \\ \bar{H}(t_{M-N+2}) \\ \vdots \\ \bar{H}(t_M) \end{bmatrix}}_{\bar{H}} \bar{X}. \tag{3.8}$$

The least square errors estimation method is applied here to compute the best estimation of $\bar{X}$ as:

$$\bar{X} = (\bar{H}^T \bar{H})^{-1} \bar{H}^T \bar{Y}. \tag{3.9}$$

Subsequently, as shown in Fig. 3.2, for the time t_{M+1}, one more pair of measurements is added and the pair of measurements at time t_{M-N+1} is removed in the equation (3.8), which yields

$$\underbrace{\begin{bmatrix} \bar{Y}(t_{M-N+2}) \\ \bar{Y}(t_{M-N+3}) \\ \vdots \\ \bar{Y}(t_{M+1}) \end{bmatrix}}_{\bar{Y}} = \underbrace{\begin{bmatrix} \bar{H}(t_{M-N+2}) \\ \bar{H}(t_{M-N+3}) \\ \vdots \\ \bar{H}(t_{M+1}) \end{bmatrix}}_{\bar{H}} \bar{X}. \tag{3.10}$$

Window Size N is the parameter which is adjustable in order to address the tradeoff between reducing the effect of noise as much as possible and keeping the track of the dynamics of Thévenin equivalents as fast as possible.

3.3.2 Recursive Least Squares Estimation with Fading Factor (RLSE)

Another state estimation method is using fading factor in recursive least squares estimation. As shown in Fig. 3.3, for recursive least squares estimation, all the measurements from the beginning are taken into account. The

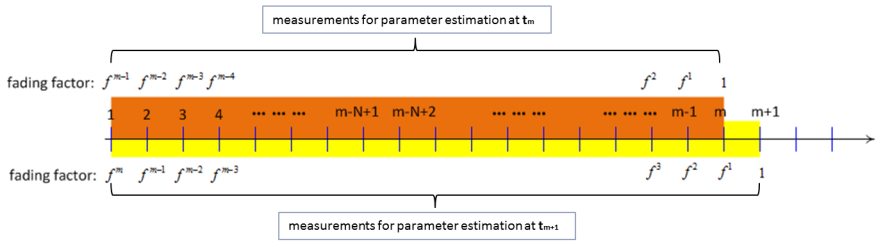

Figure 3.3: Power system stability assessments.

equation is

$$\underbrace{\begin{bmatrix} \bar{Y}(t_1) \\ \bar{Y}(t_2) \\ \vdots \\ \bar{Y}(t_M) \end{bmatrix}}_{\bar{Y_M}} = \underbrace{\begin{bmatrix} \bar{H}(t_1) \\ \bar{H}(t_2) \\ \vdots \\ \bar{H}(t_M) \end{bmatrix}}_{\bar{H_M}} \underbrace{\bar{X}}_{\bar{X}_M}. \tag{3.11}$$

When a new pair of measurements is obtained, one line is added in the matrix of equation (3.11).The equation becomes

$$\underbrace{\begin{bmatrix} \bar{Y}(t_1) \\ \bar{Y}(t_2) \\ \vdots \\ \bar{Y}(t_M) \\ \bar{Y}(t_{M+1}) \end{bmatrix}}_{\bar{Y_{M+1}}} = \underbrace{\begin{bmatrix} \bar{H}(t_1) \\ \bar{H}(t_2) \\ \vdots \\ \bar{H}(t_M) \\ \bar{H}(t_{M+1}) \end{bmatrix}}_{\bar{H_{M+1}}} \underbrace{\bar{X}}_{\bar{X}_{M+1}}. \tag{3.12}$$

The parameters $\bar{X}_{M+1}$ can also be obtained using least square errors method as

$$\bar{X}_{M+1} = (\bar{H}_{M+1}^T \bar{H}_{M+1})^{-1} \bar{H}_{M+1}^T \bar{Y}_{M+1}. \tag{3.13}$$

Consider $\bar{X}_M = (\bar{H}_M^T \bar{H}_M)^{-1} \bar{H}_M^T \bar{Y}_M$; the equation (3.13) can be derived in a recursive way as

$$\bar{X}_{m+1} = \bar{X}_m + \underbrace{\bar{Q}_{m+1}^{-1} \bar{h}_{m+1}^T}_{KalmanGain} \underbrace{(\bar{y}_{m+1} - \bar{h}_{m+1} \bar{X}_m)}_{innovations}, \tag{3.14}$$

where the quantity $\bar{Q}_{m+1}^{-1}\bar{h}_{m+1}^T$ is called the *Kalman gain*, $\bar{y}_{m+1} - \bar{h}_{m+1}\bar{X}_m$ is called *innovations* and

$$\bar{Q}_{m+1} = \bar{H}_{m+1}^T\bar{H}_{m+1} = \sum_{i=1}^{m+1} \bar{h}_i^T\bar{h}_i = \bar{Q}_m + \bar{h}_{m+1}^T\bar{h}_{m+1}. \tag{3.15}$$

By recursively estimating the parameters, the number of calculations has been reduced largely. To avoid the Kalman gain going to zero, the fading factor f is applied to give more weight to the recent measurements, as shown in Fig. 3.3. The equation (3.12) becomes

$$\underbrace{\begin{bmatrix} f^m \cdot \bar{Y}(t_1) \\ f^{m-1} \cdot \bar{Y}(t_2) \\ \vdots \\ f \cdot \bar{Y}(t_M) \\ 1 \cdot \bar{Y}(t_{M+1}) \end{bmatrix}}_{\bar{Y'_{M+1}}} = \underbrace{\begin{bmatrix} f^m \cdot \bar{H}(t_1) \\ f^{m-1} \cdot \bar{H}(t_2) \\ \vdots \\ f \cdot \bar{H}(t_M) \\ 1 \cdot \bar{H'}(t_{M+1}) \end{bmatrix}}_{\bar{H_{M+1}}} \underbrace{\bar{X}}_{\bar{X}_{M+1}}. \tag{3.16}$$

Then, the estimation equation (3.14) becomes

$$\bar{X}_{m+1} = \bar{X}_m + \underbrace{\bar{Q}_{m+1}^{-1}\bar{h}_{m+1}^T}_{KalmanGain}\underbrace{(\bar{y}_{m+1} - \bar{h}_{m+1}\bar{X}_m)}_{innovations}, \tag{3.17}$$

where

$$\bar{Q}_{m+1} = f\bar{Q}_m + \bar{h}_{m+1}^T\bar{h}_{m+1}. \tag{3.18}$$

The recursive expression can reduce the computation time. However, even with the fading factor, the incorporation of all the previous measurements leads to the lag on the modification of the *dynamic* parameters. The system parameters in the very beginning have been changed, so there is no point in still utilizing the measurements in the very beginning to estimate the current parameters.

3.3.3 Recursive Least Square Estimation with Moving Window and Fading Factor

The RLSE method seems promising in terms of calculation speed and performance; however, as discussed in the last Section 3.3.2, this method is not

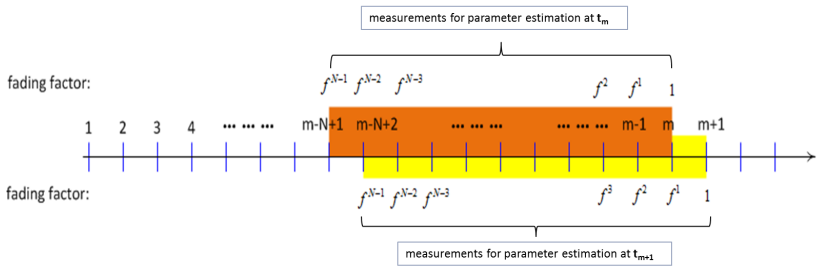

Figure 3.4: Power system stability assessment approaches.

perfect considering the dynamic characteristics of parameters. But the idea of "recursive" and fading factor can be applied to LSEMW method. The modified method can be illustrated in Fig. 3.4. The equation can be expressed as

$$\underbrace{\begin{bmatrix} f^{N-1}\cdot\bar{y}(t_{m-N+1}) \\ f^{N-2}\cdot\bar{y}(t_{m-N+2}) \\ \vdots \\ f\cdot\bar{y}(t_{m-1}) \\ 1\cdot\bar{y}(t_m) \end{bmatrix}}_{\bar{Y}'} = \underbrace{\begin{bmatrix} f^{N-1}\cdot\bar{h}(t_{m-N+1}) \\ f^{N-2}\cdot\bar{h}(t_{m-N+2}) \\ \vdots \\ f\cdot\bar{h}(t_{m-1}) \\ 1\cdot\bar{h}(t_m) \end{bmatrix}}_{\bar{H}'} \bar{X}. \tag{3.19}$$

When new pair of measurements are obtained, the equation becomes

$$\underbrace{\begin{bmatrix} f^{N-1}\cdot\bar{y}(t_{m-N+2}) \\ f^{N-2}\cdot\bar{y}(t_{m-N+3}) \\ \vdots \\ f\cdot\bar{y}t_m \\ 1\cdot\bar{y}(t_{m+1}) \end{bmatrix}}_{\bar{Y}'} = \underbrace{\begin{bmatrix} f^{N-1}\cdot\bar{h}(t_{m-N+2}) \\ f^{N-2}\cdot\bar{h}(t_{m-N+3}) \\ \vdots \\ f\cdot\bar{h}(t_m) \\ 1\cdot\bar{h}(t_{m+1}) \end{bmatrix}}_{\bar{H}'} \bar{X}. \tag{3.20}$$

The unknown parameters can be estimated in a recursive manner as

$$\begin{aligned} \bar{X}_{m+1} &= \bar{X}_m + \bar{Q}_{m+1}^{-1}[\bar{h}_{m+1}^T(\bar{y}_{m+1} - \bar{h}_{m+1}\bar{X}_m) \\ &\quad - f^{2N}\bar{h}_{m-N+1}^T(\bar{y}_{m-N+1} - \bar{h}_{m-N+1}\bar{X}_m)], \end{aligned} \tag{3.21}$$

where

$$\bar{Q}_{m+1} = f^2\bar{Q}_m + \bar{h}_{m+1}^T\bar{h}_{m+1} - f^{2N}\bar{h}_{m-N+1}^T\bar{h}_{m-N+1}. \tag{3.22}$$

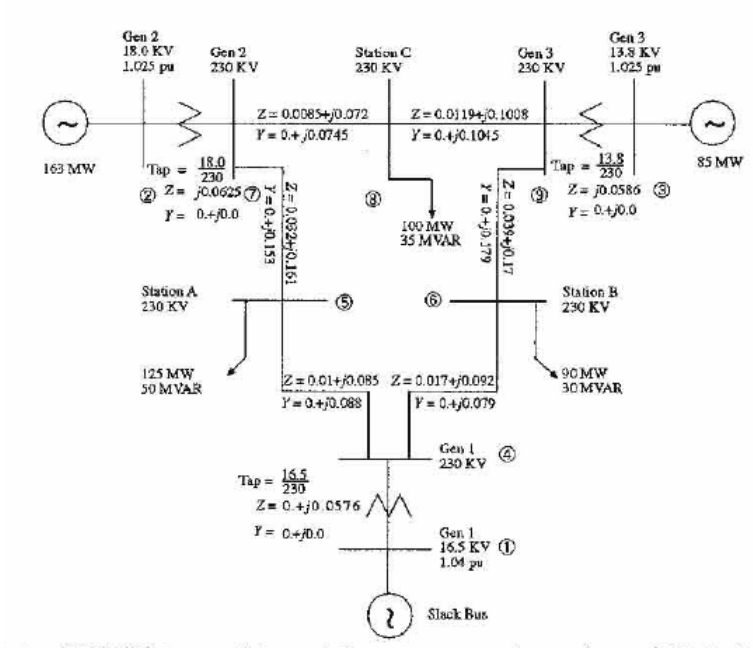

Figure 3.5: WSCC system [16].

This new method reserves the advantage of fast computation speed, assigns lower weights to the older measurements, and also eliminates the impact of the very old measurements out of the time window. Eventually, it can track the parameters more accurately while addressing the noise issue properly.

3.4 Case Study

To demonstrate the performance of this voltage stability assessment method, the 3-machine 9-bus WSCC system is simulated using PowerWorld. Figure 3.5 shows the system one line diagram (parameter values can be found in [17]). From the base case, we increase the loads in increments of 0.1% at each time point until the system collapses. Assume we set a PMU to collect the voltage and current measurements on bus 6 at each time point. Based on these measurements, we can calculate the corresponding Thevenin and load impedances at bus 8, which are shown with yellow dashed and blue solid plots respectively in Fig. 3.6. This figure demonstrates that when the system blacks out, the Thevenin impedance is approximately equal to the load impedance, which is consistent with the analysis in Section 3.2. Similarly, expected results are obtained for bus 5 and 8 (see Fig. 3.7).

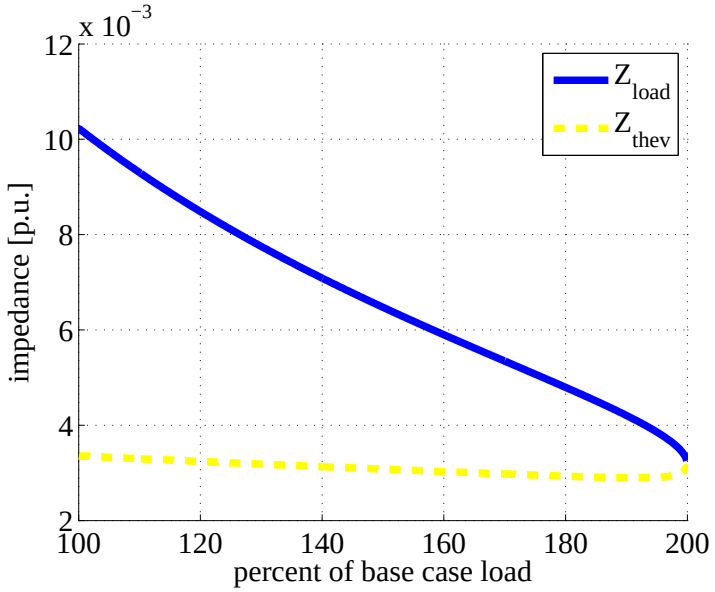

Figure 3.6: Load and Thévenin impedances at bus 6.

3.5 Chapter Summary

In this chapter, assessing system voltage stability level by utilizing PMU measurements is addressed. The methodology to estimate Thévenin equivalent parameters based on PMU measurement is presented. Building on that, system voltage stability is measured in terms of the closeness of load and Thévenin impedances. Next, data processing techniques are described to address the noise in the PMU measurements. Case studies have validated this methodology. The topics presented in this chapter are considered the background knowledge for the following work in this thesis.

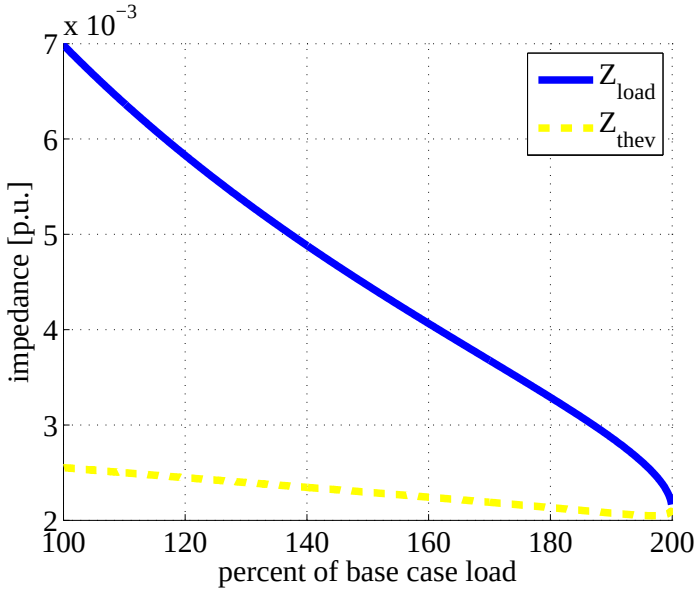

(a) Load and Thévenin impedances at bus 5.

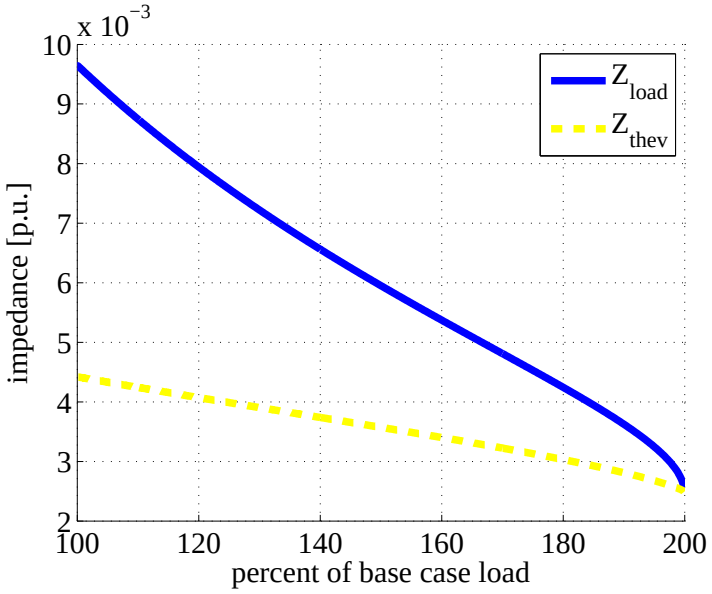

(b) Load and Thévenin impedances at bus 8.

Figure 3.7: Load and Thévenin impedances.

Chapter 4

ANGLE STABILITY

4.1 Introduction

In this chapter, the TE method is utilized to assess the system stability margin from the perspective of angle stability. Angle stability analysis provides more information about the entire system security, while voltage stability analysis focuses more on the load profiles.

However, the preliminary studies indicate that the parameter estimation methods in last chapter do not work as expected. The reason is that the assumptions used in voltage stability analysis do not apply here [18]. Therefore, the assumptions made in the TE model for angle stability analysis need to be modified. Subsequently, the TE parameter estimation equations will be different.

The rest of this chapter is organized as follows. The modeling framework is presented in Section 4.2. Section 4.3 describes the proposed stability assessment method. Section 4.4 illustrates the assessment method with examples. A couple of discussions on this method application are conducted in Section 4.5. Concluding remarks are presented in Section 4.6.

4.2 Modeling Framework

Consider a two-area system which is interconnected by a transmission line (Fig. 4.1). Two PMUs are installed at the two ends of the transmission line to collect all the phasor measurements, including the voltages on two terminals of the transmission line ($\overline{V}_1$, $\overline{V}_2$) and the currents following into the two terminals of the transmission line ($\bar{I}_1$, $\bar{I}_2$). The phasor measurements are expressed in polar form as follows:

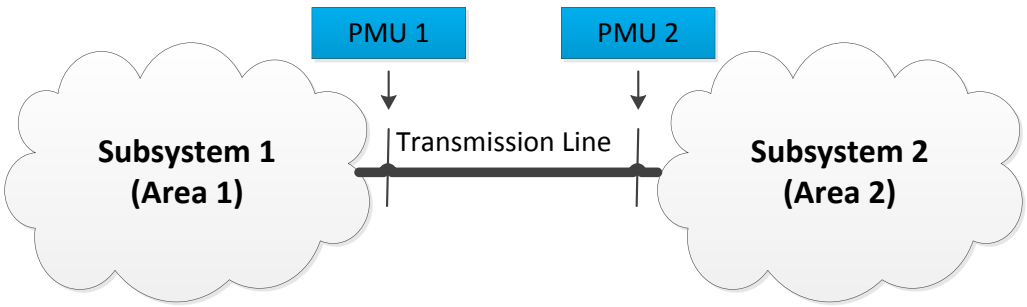

Figure 4.1: A two-area power system.

$$\begin{aligned} \bar{V}_i &= V_i\angle\theta_i,\ i = 1, 2 \\ \bar{I}_i &= I_i\angle\gamma_i,\ i = 1, 2. \end{aligned} \tag{4.1}$$

The topology and parameters inside the two subsystems are not available. However, as we know, Thévenin's theorem guarantees that linear electrical networks can be equivalent to TE circuits. For a short period of time, we can assume that the power system can be described by a linear model. Therefore, the two subsystems in Fig. 4.1 can be equivalent to two TE circuits. The transmission line can also be modeled as equivalent π circuit [19]. Then the whole system can be equivalent to the circuit shown in Fig.4.2 with TE parameters $(\bar{E}_1, \bar{E}_2, \bar{Z}_{th,1}, \bar{Z}_{th,2})$. For convenience, TE voltage sources are expressed in polar form and TE impedances are expressed in Cartesian coordination system:

$$\begin{aligned} \bar{E}_i &= E_i\angle\delta_i, \quad i = 1, 2 \\ \bar{Z}_{th,i} &= R_{th,i} + jX_{th,i}, \quad i = 1, 2. \end{aligned} \tag{4.2}$$

Now the problem is formulated to estimate the TE parameters (i.e., $\bar{E}_1$, $\bar{Z}_{th,1}$, $\bar{E}_2$, $\bar{Z}_{th,2}$) based on the PMU measurements (i.e., $\bar{V}_1, \bar{I}_1, \bar{V}_1, \bar{I}_1$).

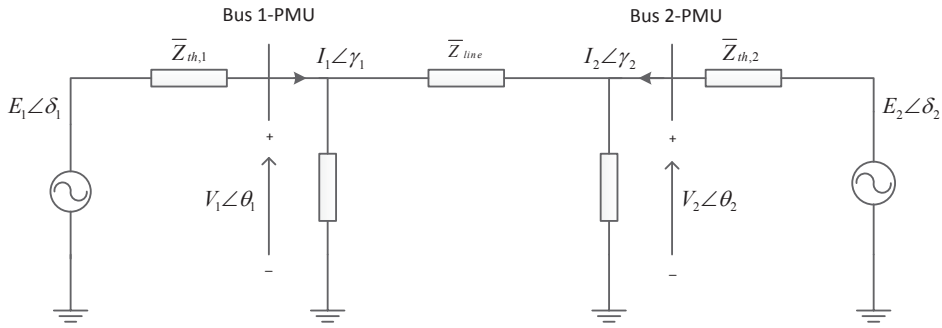

Figure 4.2: Two-area TE system.

4.3 Stability Assessment Method

4.3.1 Thévenin Equivalent's Parameter Estimation

Since the two TE circuits in Fig. 4.2 have the same structure as the TE circuit in the previous chapter for the voltage stability, the first intuition would be to use the same method to estimate the parameters; however, the results are not as expected. The reason for the unexpected results is that the assumptions made in the previous chapter do not hold for the system discussed in this chapter.

The assumption made in the previous chapter is that the parameters of TE circuits can be treated as constant compared to the rest of the system. This assumption is acceptable for voltage stability analysis since the load change is the main source of changes for the system discussed in the previous chapter. However, for the system discussed in this chapter, the rest of the system, other than the TE circuits, is the transmission line, whose change can be neglected. The main source of changes is from the TE circuits inside. Therefore we cannot assume the parameters of TE circuits are constant any more. New assumptions about TE circuits need to be introduced. Here we adopt the generator's classical model to model the TE voltage source, which implies that the time scale of the TE voltage source angle δ is much smaller than the time scale of the TE voltage source magnitude E. In this way, the angle of TE voltage source δ is a time-dependent variable rather than a constant and $R_{th} = 0$ since the resistance is assumed negligible [17]. Based on Kirchoff's voltage law, with PMU measurements at two time points t_1

and t_2, we have that

$$\begin{aligned} E_i\angle\delta_i(t_1) &= \bar{V}_i(t_1) + \bar{I}_i(t_1)\cdot\bar{Z}_{th}(t_1), \quad i=1,2 \\ E_i\angle\delta_i(t_2) &= \bar{V}_i(t_2) + \bar{I}_i(t_2)\cdot\bar{Z}_{th}(t_2), \quad i=1,2. \end{aligned} \tag{4.3}$$

From (4.3), the reactance (X_{th}) equation is derived as follows:

$$\begin{aligned} (I(t_1)^2 - I(t_2)^2)X_{th}^2 + [2I(t_1)V(t_1)\sin(\theta(t_1)-\gamma(t_1)) - \\ 2I(t_2)V(t_2)\sin(\theta(t_2)-\gamma(t_2))]X_{th} + (V(t_1)^2 - V(t_2)^2) = 0. \end{aligned} \tag{4.4}$$

Let

$$\begin{aligned} a &= I(t_1)^2 - I(t_2)^2 \\ b &= 2I(t_1)V(t_1)\sin(\theta(t_1)-\gamma(t_1)) - 2I(t_2)V(t_2)\sin(\theta(t_2)-\gamma(t_2)) \\ c &= V(t_1)^2 - V(t_2)^2. \end{aligned}$$

Then

$$X_{th} = \frac{-b \pm \sqrt{b^2-4ac}}{2a}. \tag{4.5}$$

After X_{th} is chosen as the positive root of (4.4), all the other parameters can be readily found by substituting X_{th} back into (4.3).

4.3.2 Angle Stability Assessment

Using the Thévenin equivalent-based model, the steady-state stability can be readily measured based on the transmission line's loadability (see, e.g., [20, 10, 21]). Define $(\delta_1 - \delta_2)$ as the angle across system (AAS). The power flowing through this system is

$$P = \frac{E_1E_2\sin(\delta_1-\delta_2)}{X_{th,1}+X_{ln}+X_{th,2}}. \tag{4.6}$$

The steady state stability margin (SM) can be measured by a function of AAS as follows:

$$SM = \frac{P_{max}-P}{P_{max}} = 1 - \sin(\delta_1-\delta_2). \tag{4.7}$$

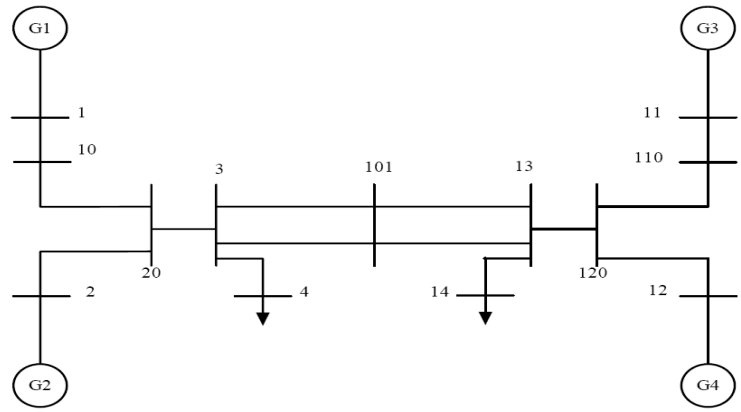

Figure 4.3: Two-area experimental system.

4.4 Case Study

To verify the modified method described above, a two-area system, as shown in Fig. 4.3 is simulated in MATLAB by using Power System Toolbox. Assume that two PMUs are set up at the terminals of the inter-area transmission line connecting bus 3 and bus 13, to measure the voltage phasors on the two buses (denoted as $\bar{V}_1(t)$ and $\bar{V}_2(t)$) and current phasors following from the two buses (denoted as $\bar{I}_1(t)$ and $\bar{I}_2(t)$). In practice, one thing that needs to be noticed is that although in this system there are two identical transmission lines between bus 3 and bus 13, these two transmission lines can be treated as one line. The voltages $\bar{V}_1(t)$, $\bar{V}_2(t)$ remain the same; the current following on the equivalent line $\bar{I}_1(t)$ is the sum of the currents flowing on those two identical transmission lines, denoted as $\bar{I}_1^{lineA}(t)$, $\bar{I}_1^{lineB}(t)$. Since $\bar{I}_1^{lineA}(t) = \bar{I}_1^{lineB}(t)$, then $\bar{I}_1(t) = \bar{I}_1^{lineA}(t) + \bar{I}_1^{lineB} = 2\bar{I}_1^{lineA}$. Based on these measurements, the Thévenin equivalents can be obtained on both sides of this transmission line. Then, the power system can be reduced to the equivalent system as shown in Fig. 4.2. And the SM can also be calculated to indicate the system stability level. In the simulations, the loads and generations are increased by 1% gradually at each time step until the system goes to collapse. In order to verify the results easily, we analyze the system when it is at nearby stability limit. Right before the system blacks out, two sets of simulated PMU measurements, $\bar{V}_1(t_1), \bar{I}_1(t_1), \bar{V}_2(t_1), \bar{I}_2(t_1)$ and $\bar{V}_1(t_2), \bar{I}_1(t_2), \bar{V}_2(t_2), \bar{I}_2(t_2)$, are collected. The values are listed in Table B.3 in Appendix B. The estimation results of Thévenin-equivalent parameters by using this method are presented in Table 4.1. The table shows that this method has a good performance as

Table 4.1: Thévenin equivalent parameter estimations

	Estimation	Improper assumptions
E_1 [p.u.]	0.9671	0.8783
E_2 [p.u.]	1.0138	1.2891
$\delta_1 - \delta_2$ [degree]	71.7282	-3.4712
SM	5%	94%
$X_{th,1}$ [p.u.]	0.1080	0.1245
$X_{th,2}$ [p.u.]	0.1349	-0.4537

expected. Although because of the 1% incremental size, the SM is not exactly 0%; the very small SM of value 5% indicates the system is in a quite intensive situation. Therefore the results have validated our assumptions made in the beginning of this chapter. To illustrate the outcome of misusing the assumptions made in Chapter 3 to angle stability analysis, we apply the method proposed in the previous chapter, which is specifically designed for voltage stability analysis to the measurements. The results are also listed in Table 4.1. The small AAS obtained, corresponding to large SM, does not reflect the system situation correctly since the system is operated about to collapse.

4.5 Further Discussion

4.5.1 Comparison with Other System Equivalencing Method

Methods regarding system equivalencing based on phasor measurements have emerged along with the popularity of PMUs. Here we compare our method with another method which is along the lines of the equivalent method as well; the details can be found in [8, 9]. The distinct point about this method is that a third middle (virtual) bus is involved to estimate the equivalent parameters. The same test system discussed in Section 4.4 is used here. We arbitrarily choose one operating state and record the measurements from PMUs. Then we change the system with a small disturbance and record another set of measurements. The estimation results from these two methods are shown in Table 4.2. Here we can see the estimated equivalent reactances from these two methods are equal to each other. Consequently, since equivalent

Table 4.2: Thévenin equivalent estimation comparison

	$X_{th,1}$ [p.u.]	$X_{th,2}$ [p.u.]
Our method	0.10	0.13
Method in [8, 9]	0.10	0.13

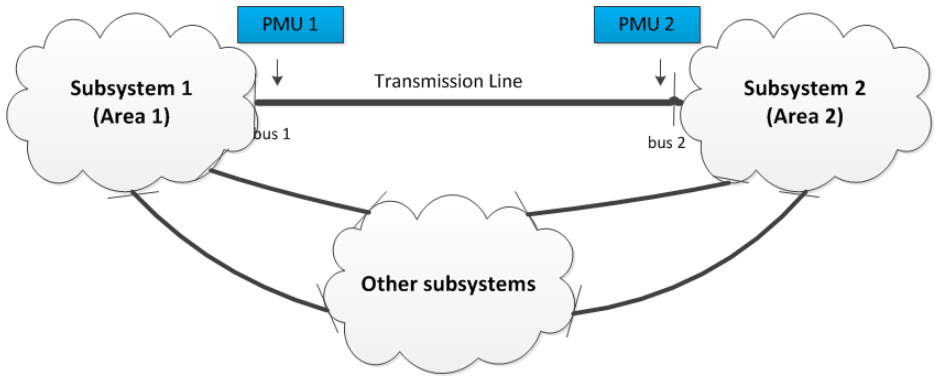

Figure 4.4: General system.

voltage is calculated as $\bar{E} = \bar{V} + \bar{I} \cdot jX_{th}$, the estimated equivalent voltage sources from two methods are equal as well. Therefore, these two methods have cross-verified each other. But the method we proposed here has fully exploited the phase information from PMU data; consequently, we avoided involving a third bus and simplified the processes.

4.5.2 Application on Meshed Systems

As discussed above, this method performs effectively with two-area systems. Next we want to broaden the applications to more complicated general systems, where two areas are interconnected through at least one more path besides the tie line of our interest, as shown in Fig. 4.4.

One simple example is as shown in Fig. 4.5, where the additional path is also a transmission line. Fortunately, we can prove that our method is still valid under the assumption that both transmission lines have same R/X ratio. The proof is as follows.

Assume that we only monitor the voltage and current phasors on transmission line A in Fig. 4.5. Let $\bar{Z}^A = k\bar{Z}^B$, $k \in \mathbb{R}^+$. Then

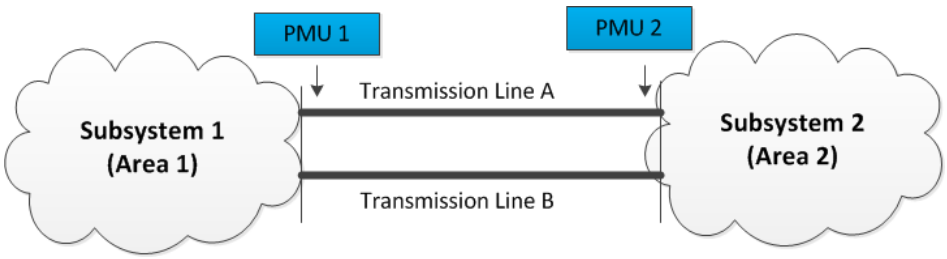

Figure 4.5: System with two transmission lines.

$$\begin{aligned} \bar{I}^A &= \frac{1}{k}\bar{I}^B \\ \bar{I} &= \bar{I}^A + \bar{I}^B = (1+\frac{1}{k})\bar{I}^A = q\bar{I}^A, \end{aligned} \tag{4.8}$$

where $q = 1 + \frac{1}{k}$.

Voltages on the same bus are the same:

$$\bar{V}^A = \bar{V}^B = \bar{V}. \tag{4.9}$$

Then by replacing the $\bar{V}$ and $\bar{I}$ in (4.4) by $\bar{V}^A$and $\bar{I}^A$, we have

$$\begin{aligned} &(I^A(t_1)^2 - I^A(t_2)^2)X_{th}^{'2} + [2I^A(t_1)V^A(t_1)\sin(\theta^A(t_1) - \gamma^A(t_1)) - \\ &2I^A(t_2)V^A(t_2)\sin(\theta^A(t_2) - \gamma^A(t_2))]X_{th}^{'} + (V^A(t_1)^2 - V^A(t_2)^2) = 0. \end{aligned} \tag{4.10}$$

By letting

$$\begin{aligned} a^A &= I^A(t_1)^2 - I^A(t_2)^2 \\ b^A &= 2I^A(t_1)V^A(t_1)\sin(\theta^A(t_1) - \gamma^A(t_1)) - 2I^A(t_2)V^A(t_2)\sin(\theta^A(t_2) - \gamma^A(t_2)) \\ c^A &= V^A(t_1)^2 - V^A(t_2)^2, \end{aligned}$$

we obtain that the solution of 4.10 is given by

$$X_{th}^{'} = \frac{-b^A \pm \sqrt{(b^A)^2 - 4a^Ac^A}}{2a^A}.$$

By applying (4.8) and (4.9), we obtain

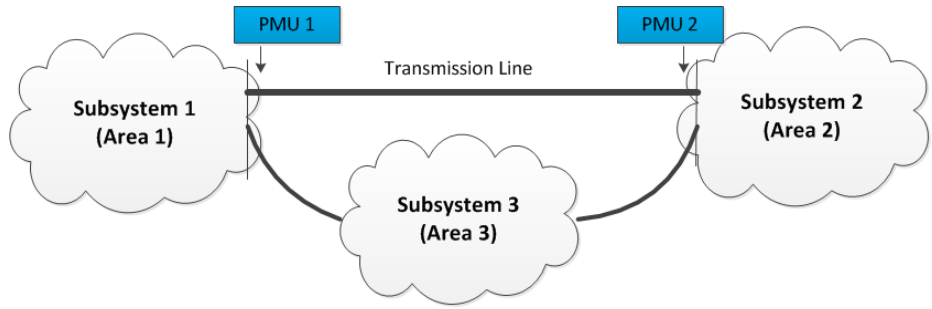

Figure 4.6: System with additional path going through a third area.

$$a^A = \frac{1}{q^2}a,\ b^A = \frac{1}{q}b,\ c^A = c,$$

and comparing with (4.5), we have

$$X'_{th} = \frac{-\frac{1}{q}b \pm \sqrt{(\frac{1}{q}b)^2 - 4\frac{1}{q^2}ac}}{2\frac{1}{q^2}a} = q\frac{-b \pm \sqrt{b^2 - 4ac}}{2a} = qX_{th}.$$

Eventually, by applying KVL,

$$\bar{E}'_{th} = \bar{V}^A + \bar{I}^A \cdot X'_{th} = \bar{V} + \frac{1}{q}\bar{I} \cdot qX_{th} = \bar{V} + \bar{I} \cdot X_{th} = \bar{E}_{th}.$$

Therefore, although the measurements from one of the parallel transmission lines are utilized, the estimation of equivalent voltage has not been reflected. Consequently, the SM will still reflect the system situation correctly.

As a case study, in the test system of section 4.4, we apply our method to the measurements from one of the two transmission lines connecting bus 3 and bus 13 (e.g., $\bar{V}_1^{lineA}(t_1), \bar{I}_1^{lineA}(t_1)$, $\bar{V}_2^{lineA}(t_1)$, $\bar{I}_2^{lineA}(t_1)$ and $\bar{V}_1^{lineA}(t_2)$, $\bar{I}_1^{lineA}(t_2)$, $\bar{V}_2^{lineA}(t_2)$, $\bar{I}_2^{lineA}(t_2)$). The results are exactly the same as in Section 4.4.

Another example is that the additional path goes through a third subsystem as shown in Fig. 4.6. Here a circuit analysis method is required to convert the system into a two-area system. A promising method is using Tellegen's theorem to analyze the network [22]. This example and the even more general case as shown in Fig 4.4, where more buses, other than the terminal buses of the tie line, are involved in the paths, remain for future work.

4.6 Chapter Summary

In this chapter, a Thévenin equivalent method for two-area one-tie line system is developed by making appropriate assumptions. Consequently, an equivalent parameter estimation method is developed. Then, based on the equivalent models, a metric SM is proposed to measure the system stability. An two-area system case is studied to illustrate the procedure and the result has verified the effectiveness of this method. After that, a comparison with other equivalencing methods is carried out to address the advantages of our method. For broader applications, we have proved that this method is valid for parallel transmission lines between two areas. The application to even more general power systems is part of our ongoing work.

Chapter 5

PMU DATA FREQUENCY DOMAIN ANALYSIS AND SYSTEM INERTIA ESTIMATION

5.1 Introduction

As mentioned in Chapter 3, in order to estimate system equivalents, the classical model is adopted [17]:

$$\begin{aligned} \frac{d\delta}{dt} &= \omega - \omega_s \\ \frac{2H}{\omega_s}\frac{d\omega}{dt} &= T_M - P_e - T_{FW} \\ &= T_M - \frac{EV_s}{X_d^{'} + X_{ep}} \sin(\delta - \theta_{vs}) - T_{FW}, \end{aligned} \tag{5.1}$$

where the equivalent TE voltage source magnitude E and equivalent reactance $X_d^{'} + X_{ep}$ have already been estimated in the last chapter. This expression enables further simulation (e.g., to simulate the system performance in the occurrence of faults) if equivalent inertia H can be estimated by utilizing PMU data [19]. Several works have applied frequency domain analysis on PMU data in the hope of extracting valuable information about the system [23]. For instance, the Prony method, which expresses PMU measurements as a linear combination of damping sinusoids with different frequencies, is applied successfully to monitor the system stability [24]. With the inspiration of this technique, we develop the method to estimate the system inertia based on the dominant frequency from frequency domain analysis.

This chapter proceeds as follows. Section 5.2 presents the fundamental knowledge of frequency domain analysis used in PMU data application. Section 5.3 describes the system inertia estimation method. Section 5.4 illustrates the proposed methodology with benchmark systems which are simulated in a real time digital simulator (RTDS) testbed. Concluding remarks

are made in Section 5.5.

5.2 Preliminaries: Frequency Domain Analysis and Frequency Spectra

Each set of PMU measurements (e.g., a set of voltage magnitude, a set of current magnitude, etc) can be viewed as a discrete signal flow. From the discrete Fourier transform (DFT), the frequency domain of a discrete signal can be expressed as

$$X(k) = \sum_{n=0}^{N-1} x(n) e^{-j(2\pi/N)kn}, \quad 0 \leq n \leq N-1. \tag{5.2}$$

The magnitude of $X(k)$ is the oscillation amplitude at frequency $\frac{kS}{N}$ ($0 \leq k < \frac{N}{2}$), where S is the PMU's sampling rate and N is the number of samples [25]. Therefore $||X(k)||$ can provide the frequency spectra of the N consecutive PMU measurements. The frequency at which the maximum magnitude happens is called the dominant frequency (DF), denoted as f_D, and the corresponding magnitude is denoted as $||X_D||$. The beauty of the power system DF is that, because it is the reflection of the system innate parameters (e.g., the system inertia), it keeps constant during disturbance for a specific power system. Therefore, DF makes it possible to estimate system inertia based on the PMU measurements, which will be illustrated in Section 5.3. Notice that during the disturbance, the observables (i.e., voltage magnitude and angle, current magnitude and angle) vary at the same DF, although with different magnitude. Therefore it is acceptable to monitor any one of the observables in order to obtain the DF.

The fast Fourier transform (FFT) technique, as an efficient algorithm to perform DFT, is deployed during the computation, which can allows for almost real time monitoring of the measurements in frequency domain [26]. As a side application, since FFT enables fast PMU data processing in the level of real time, the oscillation amplitude at dominant frequency along with time $||X_D(t)||$ can be used as a system performance index to monitor the system stability in real time. In the frequency domain, if the amplitude

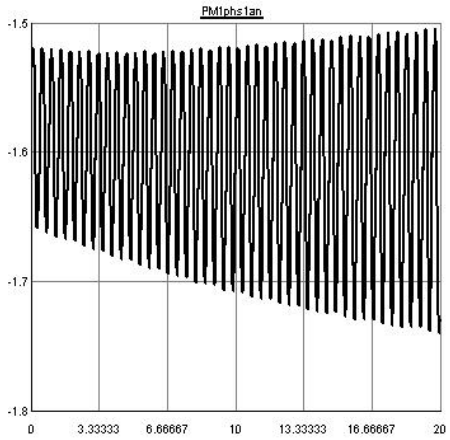

(a) The angle of voltage phasor along with time.

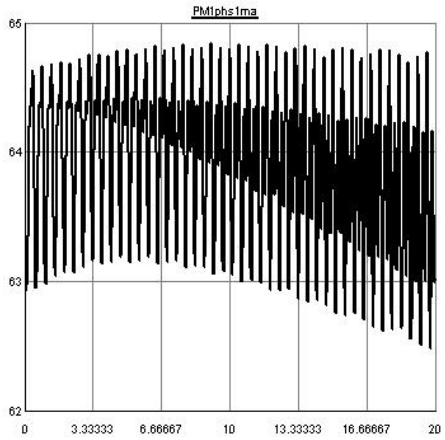

(b) The magnitude of voltage phasor along with time.

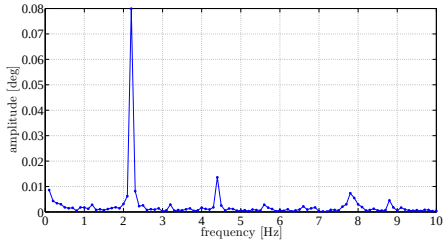

(c) Frequency spectra of voltage angle.

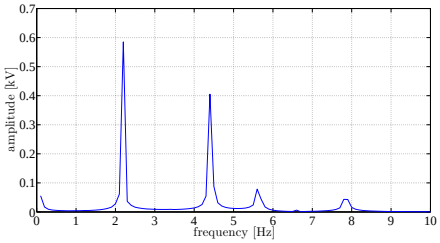

(d) Frequency spectra of voltage magnitude.

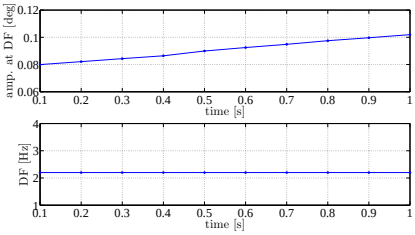

(e) Dominant frequency of voltage angle and its magnitude along with time.

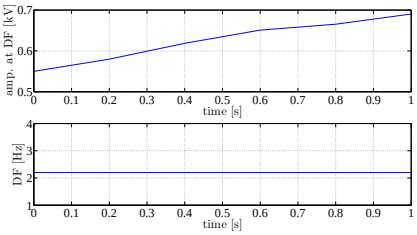

(f) Dominant frequency of voltage magnitude and its magnitude along with time.

Figure 5.1: Voltage phasor FFT analysis.

at dominant frequency $||X_D(t)||$ increases without bounds, it is an indication of transient instability.

We illustrate the application of frequency domain analysis introduced above with the following example. The power system is simulated in a real time digital simulator testbed, which is described in detail in Section 5.4.1. The power system frequency domain features are also demonstrated in this example.

Example 1: Consider a two-bus system, consisting of a generator connected to one bus and a load connected to the other bus. The generator is comprehensively simulated by the multi-time scale model (see [17] for the model description), with IEEE Type 2 stabilizer, IEEE Type ST1 excitation system and IEEE Type 2 turbine/governor (see [27] and [28] for details).

We vary the load to create disturbances. The observables (i.e., voltage angle and magnitude, current phasors and frequency) are measured by the PMU and recorded in Fig. 5.1a, 5.1b, 5.2a, and 5.2b, respectively . The magnitudes of currents and voltages are not the real values and subject to the ratio of current transformers and potential transformers. However, in this method, the exact values of the currents and voltages are not critical; therefore, the ratio does not affect the final results.

FFT is applied to each observable and the frequency spectra for the first 200 measurements are respectively plotted in Fig. 5.1c, 5.1d, 5.2c and 5.2d, respectively. As expected, the dominant frequencies are the same for all observables as 2.2 Hz. The dominant frequencies and their amplitudes along with time are respectively plotted in Fig. 5.1e, 5.1f, 5.2e and 5.2f. We can see that the dominant frequency keeps constant through all the time across all observables. Particularly, for this case, we can also conclude from the increasing amplitudes that this monitored system is unstable and proper protective action is required.

Next we increase the inertia of the generator and repeat the same procedure above. Without loss of generality, we take one observable (i.e., frequency) as an instance, whose measurements are plotted in Fig. 5.3a. Its frequency spectra of the first 200 points, and the dominant frequency along with time, are respectively plotted in Fig. 5.3b and 5.3c, where we can see the stationary property of DF holds as well. Other sets of figures for the remaining observables are given in Appendix C. In this case, the increased inertia decreases the dominant frequency. The conclusion can be reached from the decreasing

amplitudes that this system becomes stable.

5.3 System Inertia Estimation

We rewrite the classical model expression as follows:

$$\begin{aligned} \frac{d\delta}{dt} &= \omega - \omega_s \\ \frac{2H}{\omega_s}\frac{d\omega}{dt} &= T_M - P_e - T_{FW}, \end{aligned} \tag{5.3}$$

where T_M is the mechanical torque, T_{FW} is a friction windage torque and P_e is the power supplied by the equivalent circuit, which is equal to $\frac{EV}{X_{th}}\sin(\delta-\theta)$ in terms of the equivalent system in Fig. 4.2.

By linearizing around an operating point, we obtain:

$$\begin{aligned} \frac{d}{dt}\Delta\delta &= \Delta\omega \\ \frac{d}{dt}\Delta\omega &= \frac{\omega_s}{2H}[\Delta T_M - \Delta P_e - \Delta T_{FW}]. \end{aligned} \tag{5.4}$$

Assume that T_M and T_{FW} are constant [17] and $\Delta P_e = \frac{\partial P_e}{\partial \delta}\Delta\delta$. We obtain

$$\frac{d}{dt}\begin{bmatrix}\Delta\delta \\ \Delta\omega\end{bmatrix} = \begin{bmatrix} 0 & 1 \\ -\frac{\omega_s}{2H}\frac{\partial P_e}{\partial \delta} & 0 \end{bmatrix}\begin{bmatrix}\Delta\delta \\ \Delta\omega\end{bmatrix} =: A\begin{bmatrix}\Delta\delta \\ \Delta\omega\end{bmatrix}. \tag{5.5}$$

Again the time scale issue needs to be addressed here. The assumption we made here is that equation (5.5) describes a time invariant system, which is acceptable for a short period. Then (5.5) is a linear second order differential equation with eigenvalues:

$$\lambda_1 = j\sqrt{\frac{\omega_s}{2H}\frac{\partial P_e}{\partial \delta}} \text{and } \lambda_2 = -j\sqrt{\frac{\omega_s}{2H}\frac{\partial P_e}{\partial \delta}}.$$

Therefore the system oscillation frequency is

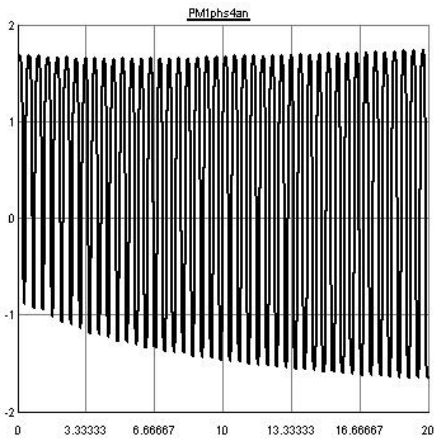

(a) The angle of current phasor along with time.

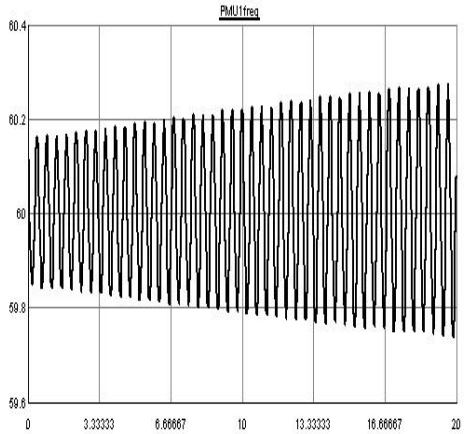

(b) Frequency along with time.

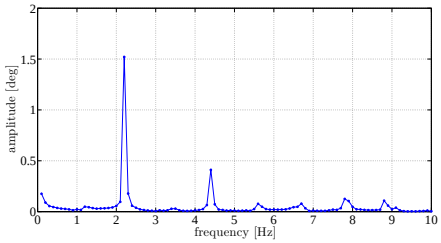

(c) Frequency spectra of current angle.

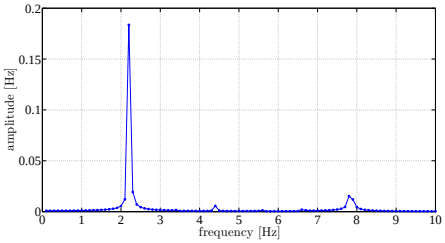

(d) Frequency spectra of frequency.

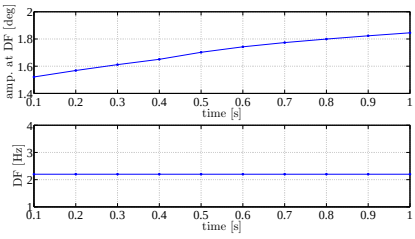

(e) Dominant frequency of current angle and its magnitude along with time.

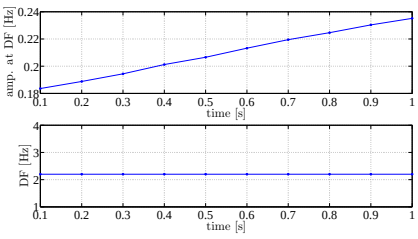

(f) DF of frequency and its magnitude along with time.

Figure 5.2: Current angle and frequency FFT analysis.

$$\omega = 2\pi f = \sqrt{\frac{\omega_s}{2H}\frac{\partial P_e}{\partial \delta}}. \tag{5.6}$$

Notice that the system oscillation frequency is actually the dominant frequency, which has been obtained by applying the frequency domain analysis on the PMU data in the previous section. Building on that, we can directly estimate the system inertia H as follows:

$$\hat{H} = \frac{\omega_s}{8\pi^2 f^2}\frac{\partial P_e}{\partial \delta} = \frac{\omega_s}{8\pi^2 f^2}\frac{EV}{X_{th}}\cos(\delta - \theta). \tag{5.7}$$

The ideas above are illustrated in the following example, which is a continuation of Example 1.

Example 2: Consider the two-bus power system discussed in Example 1. For the first case, the dominant frequency is 2.2 Hz as shown in Fig. 5.2. Using equation (5.7), the estimated inertia ($\hat{H}$) is calculated as 1.713 Hz, which is close to the generator's inertia value H that has been set up in RTDS as 1.7 Hz. The closeness of estimated and real inertias verifies that the classical model is enough to capture the system dynamics in terms of inertia estimation.

5.4 Case Study

In this section, we use the methodology described in the previous sections to analyze the two-area power system discussed in the previous chapter. The testbed setup is described in the following. Then, based on the PMU measurements from the testbed, the frequency domain analysis and equivalent inertia estimation are proceeded as follows.

5.4.1 Testbed Description

To mimic the real world situation to the utmost (e.g., to take into account the noise generated by the real PMUs), the experiment is performed in a

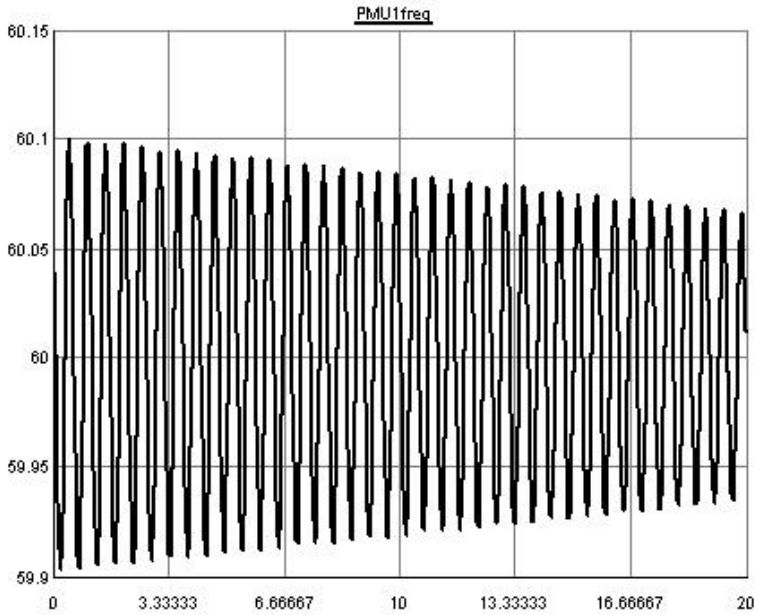

(a) Frequency along with time.

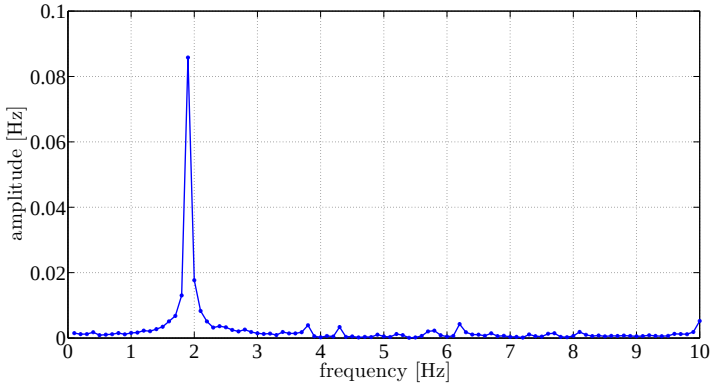

(b) Frequency spectra of frequency.

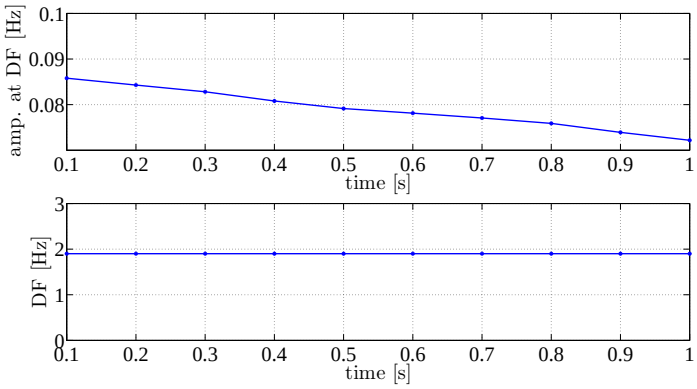

(c) DF of frequency and its magnitude along with time.

Figure 5.3: Frequency FFT analysis for a different system.

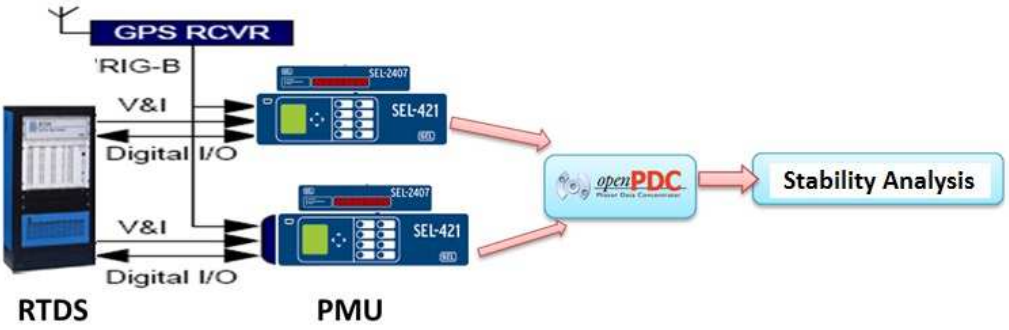

(a) RTDS/PMU/PDC testbed configuration.

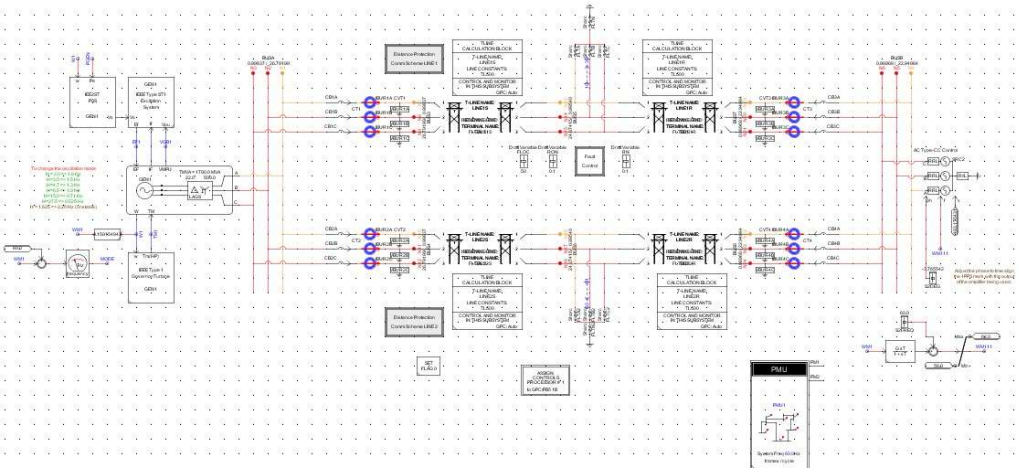

(b) RSCAD power system oneline diagram.

Figure 5.4: RTDS simulated power system.

testbed consisting of a real time digital simulator (RTDS), two phasor measurement units (PMUs) and a phasor data concentrator (PDC). The RTDS simulator is designed specifically to simulate electrical power systems. It solves electromagnetic transient simulations in real time and provides flexible interconnections with PMUs to supply the values of voltages and currents of interest. Oneline diagrams of the power systems can be easily created and modified in RSCAD, which is a user-friendly interface with the RTDS hardware [29]. SEL-421 Protection, Automation, and Control System is applied in our testbed to perform the PMU functions [30]. The testbed configuration and an one-line power system diagram example created in RSCAD are presented in Fig. 5.4a and 5.4b, respectively. As depicted in Fig.5.4a, the system is simulated in RTDS; the voltage and current measurements on each bus are sent out to one PMU. Then, the phasor data obtained from PMUs are collected in PDC for analysis. Fig. 5.4b depicts the one-line diagram representing the power system analyzed in Example 1 and 2.

5.4.2 Two-Area System Analysis Results

As a continuation of Section 4.4, the two-area system as shown in Fig. 4.3 is studied in this section. Without loss of generality, we take the left PMU on bus 3 as an instance. When the load is varied and disturbance occurs, the PMU measurements, frequency domain and dominant frequency along with time are plotted in Fig. 5.5. The dominant frequency stays at 0.6 Hz. It is obvious that with this load disturbance the system is still stable, which is consistent with the decreasing amplitude at the DF. Using equation (5.7), the estimated inertia is calculated as 30.32 p.u.

5.5 Chapter Summary

In this chapter, the frequency domain analysis and dominant frequency concept are first introduced. Building on that, system equivalent inertia estimation methodology is developed. Combining with the previous chapter, all the parameters of the system equivalents are available, which makes possible real-time stability monitoring, assessment and fault analysis based on this simplified equivalent model. A RTDS/PMU/PDC testbed is utilized to

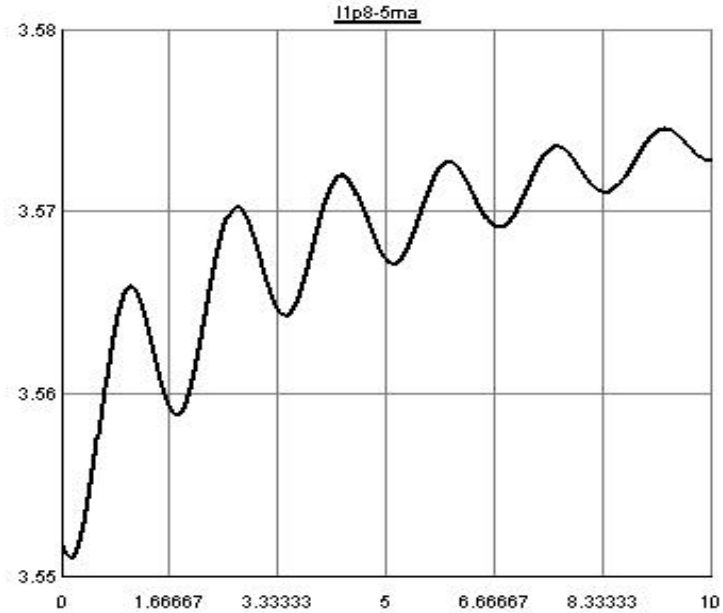

(a) The magnitude of current phasor along with time.

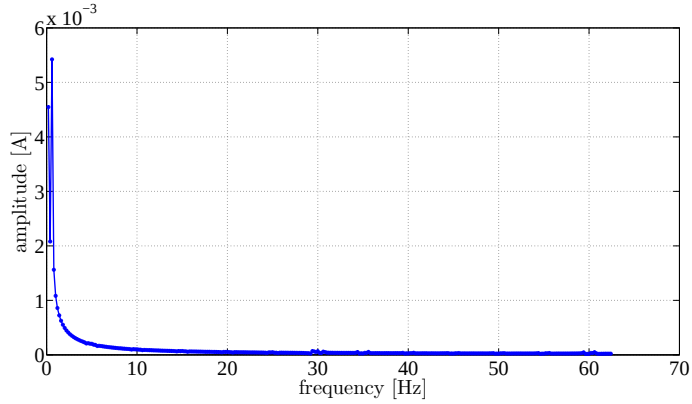

(b) Frequency spectra for the first 250 sample points.

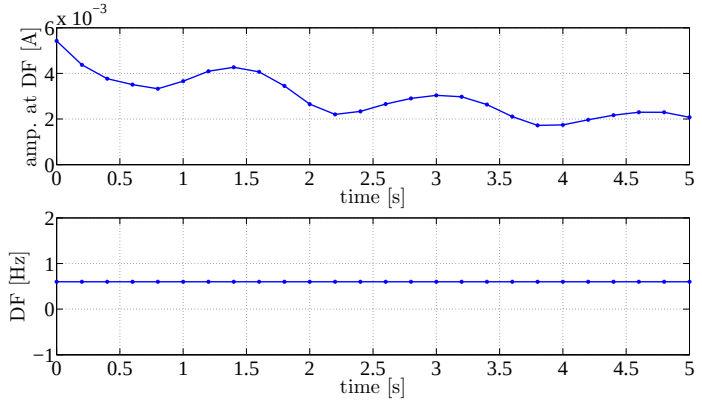

(c) Dominant frequency and its magnitude along with time.

Figure 5.5: Current phasor FFT analysis.

simulate power systems in this chapter. A two-bus system is analyzed as an example to demonstrate the constant dominant frequency feature and to illustrate the procedures. A two-area system is demonstrated and the results have validated the equivalent inertia estimation method. Further applications of the equivalent technique will be presented in a series of real case studies in the next chapter.

Chapter 6

REAL POWER SYSTEM CASE STUDIES

6.1 Introduction

In this chapter, We apply the methodology described in Chapters 3-5 to two sets of PMU measurements which are recorded from two separate transmission systems and provided by two independent transmission system operators. The procedures, partial results and observations are presented as follows.

Each power transmission system has the same PMU setup as described in Chapter 4, which is replotted here in Fig. 6.1. Two PMUs are set up at the two terminals of a main tie line to measure the voltage and current phasors. In case 1, the tie line is 345 kV, while for case 2, the tie line is 756 kV. Because of different PMU configurations, some PMUs measure the real powers, reactive powers and voltage phasors, rather than voltage and current phasors. Then current phasors need to be calculated out using

$$\bar{I} = \left(\frac{\bar{S}}{\bar{V}}\right)^* .$$

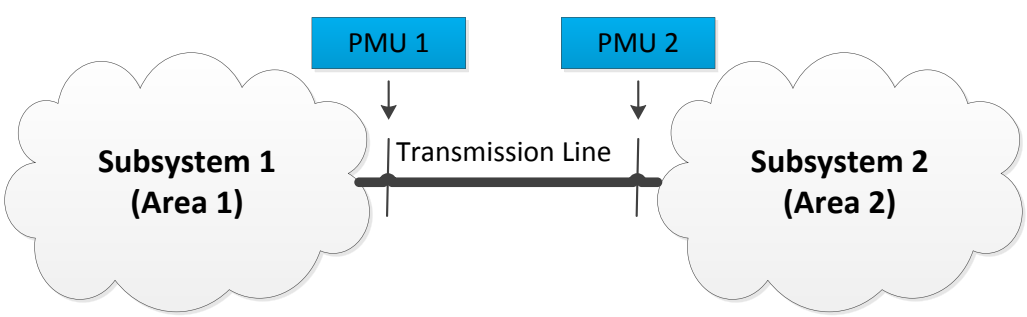

Figure 6.1: Power system structure.

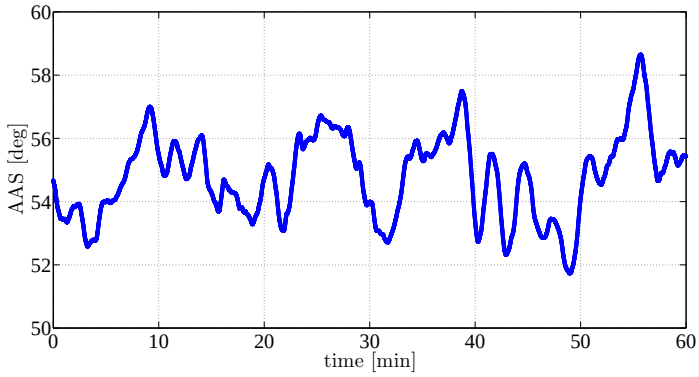

Figure 6.2: AAS of case 1.

6.2 Case 1: 345 kV Transmission System

The tie line in the first power system is a 345 kV line. The synchronized phasor data are recorded by two PMUs set up at the two terminals of this tie line.

6.2.1 System Steady-State Angle Stability

The algorithm developed in Chapter 4 is applied to this set of PMU measurements. As stated in Chapter 4, the equivalent system as shown in Fig. 4.2 is derived. To illustrate the result, we arbitrarily choose one hour period. The Angle Across System (AAS), as a system stability index, is plotted along with time in Fig. 6.2. Here we can conclude during this period, the system is relatively safe in terms of system angle stability, since the stability margin (SM) (defined by $SM = 1 - \sin(AAS)$) is around 23.4%.

The PMUs have measured the voltages and currents for a whole day. By analyzing these measurements, the observations are presented as follows.

- The steady-state stability margin can provide a valid index to reflect the system situation. For instance, a small stability margin occurs during the 2:00 pm to 3:00 pm when the tie line is heavily loaded.

- The steady-state stability margin also provides a quantitative measure of how far the system is from instability (i.e., the maximum line loadability). The maximum line loadability in terms of steady-state

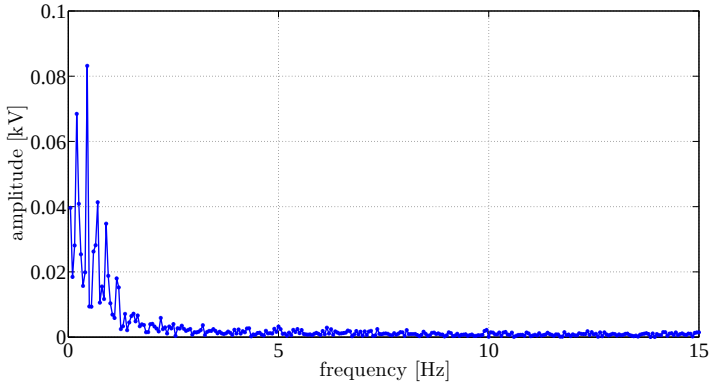

(a) Frequency spectra of voltage magnitude.

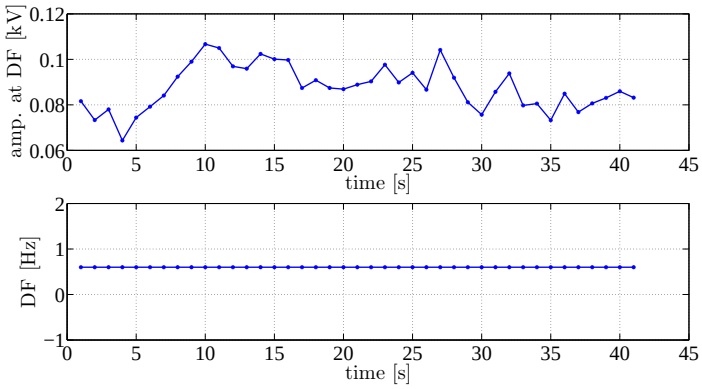

(b) Dominant frequency and its magnitude along with time.

Figure 6.3: Dynamic analysis of case 1.

stability is generically smaller than the thermal limit of the transmission line. Therefore SM gives a more accurate index about the system situation to operators.

- The PMU data quality is still an ongoing research area. In this case, PMU data missing and bad data happen quite often, which, as well as the measurement noises, requires a relatively large window size during the parameter estimation.

- The time scale is another factor to be considered. Practically the window size should be chosen based on the system specific inertia characteristics. Also, generically the time scale of dynamic analysis is smaller than that of steady-state analysis. Consequently, dynamic analysis has a higher requirement on data quality.

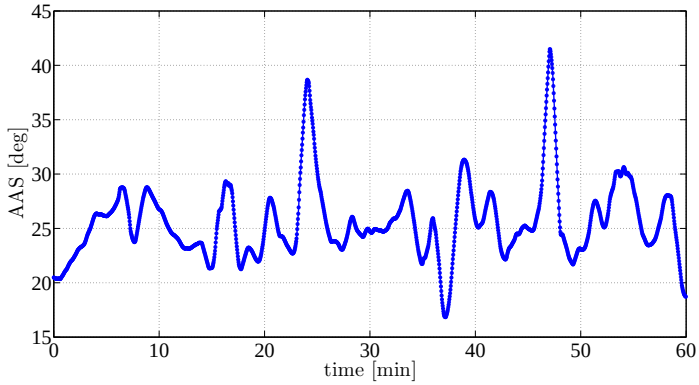

Figure 6.4: AAS of case 2.

6.2.2 System Dynamic Analysis and Equivalent Inertia Estimation

We apply the methodology developed in Chapter 5 to this system. For a certain period, the frequency spectra for the measurements of the first 600 sample points are shown in Fig. 6.3a. During the whole period, the dominant frequency (DF) and corresponding magnitude along with time are plotted in Fig. 6.3b. From the figure, we can observe that during this period, the system's DF is 0.6 Hz, which, as expected, remains constant. Consequently, the system equivalent inertia is calculated to be 31.8719 p.u. using equation 5.7. In addition, we can observe that the corresponding amplitude at the dominant frequency is bounded, which indicates that the system is stable in terms of dynamic stability during this period.

6.3 Case 2: 756 kV Transmission System

The second power system we studied consists of one 756 kV tie line and the synchronized phasor data are recorded by two PMUs set up at the two terminals of this tie line. Same procedures are performed as case 1.

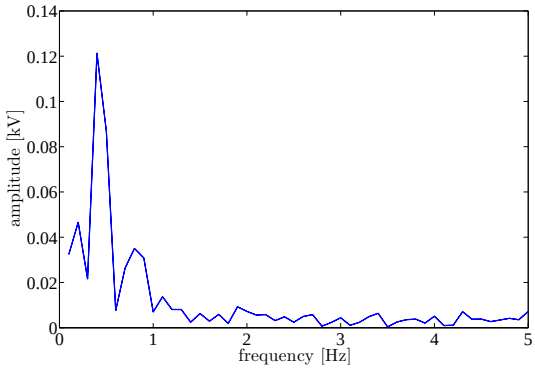

(a) Frequency spectra.

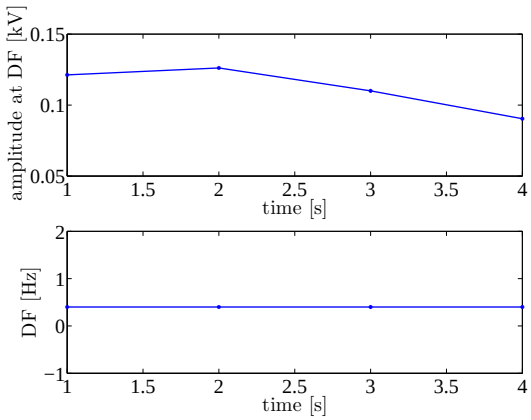

(b) Dominant frequency and its magnitude along with time.

Figure 6.5: Dynamic analysis of case 2.

6.3.1 System Steady-State Angle Stability

For a one hour period, the angle across system (AAS), as a system stability index, is plotted along with time in Fig. 6.4. We can conclude that, during this period, the system is relatively safe in terms of system angle stability, since the stability margin (SM) is around 54.6%. Then we can further conclude that the second system is less stressed than the first system in Section 6.2, even though these two systems have different ratings.

6.3.2 System Dynamic Analysis and Equivalent Inertia Estimation

For a certain period, the frequency spectra for the PMU measurements of the first 600 sample points are plotted in Fig. 6.5a. The DF and corresponding

magnitude along with the whole period are depicted in Fig. 6.5b. The system DF stays constant at 0.4 Hz. This is reasonable since this system has a higher rating than the first system. We can also conclude that the system is stable in terms of dynamic stability based on the decreasing magnitude at DF.

Chapter 7

CONCLUSIONS AND FUTURE WORK

This thesis proposes a systematic framework for system stability analysis by utilizing PMU measurements. The motivation is rooted in system equivalencing ideas. According to the Thévenin theorem, an electrical system with two terminals can be equivalent to a highly reduced system (a combination of a voltage source and an impedance in series). The parameters in the equivalent models can be estimated using PMU data due to PMUs' high time resolution and synchronizing measure ability. Eventually, the system stability can be assessed by analyzing the equivalent system. The main merits of this equivalent system-based stability analysis methodology can be summarized as follows:

- The equivalent model is simple and easy to understand, which results in small number of unknown parameters and consequentially small computation volume. Meanwhile, the accuracy is guaranteed due to the equivalent theory.
- This method is purely based on measurements. The network topology is not required. Therefore, this method can be implemented locally, for instance, at the substation level.
- Due to model simplicity and the topology-less property, this method is so computationally effective that it allows online real-time applications. Consequentially, remedial actions can be taken more quickly if the system goes unstable.

In particular, both voltage stability and angle stability are investigated in this thesis in terms of steady state. The voltage stability is specifically for load bus, while steady-state angle stability analysis, based on the system loadability, focuses on general transmission systems with tie line. Next, we extend further to dynamic analysis. Frequency domain analysis is introduced

and the results can be used for unstable oscillation awareness. More essential, the last parameter, equivalent inertia of the dynamic model, can be estimated based on the frequency domain analysis result. The main conclusions from the studies are as follows:

- As the most mature application of PMU measurements, voltage stability analysis fully utilizes the phasor information and demonstrates good performance in the stability assessment.

- Stability margin can be obtained based on the angle stability analysis. The PMU configuration to implement this algorithm is so simple that it allows on-line and local application.

- To make the most use of the high resolution provided by the high PMU sampling frequency, frequency domain analysis provides a good tool to mine the PMU data. It has been observed that during small disturbances, the dominant frequency, corresponding to the largest amplitude oscillation, would keep constant. Next, this property can be used to estimate the system equivalent inertia.

Future work will be conducted in the following aspects:

- Parameter estimation method is the foundation of this equivalent-based stability assessment methodology. How to properly choose the window size and fading factor still relies on experience. Theoretical analysis on the optimal window size and fading factor will be an interesting direction to pursue.

- It has been proven that the angle stability assessment method is applicable to systems with parallel tie lines. Extending this angle stability assessment method into a more general, meshed system, is still under investigation.

- All the parameters for the classical model have been estimated. Next, analytical transient stability methods (e.g., energy function methods) can be easily applied to the equivalent systems.

- For the real power system cases, studies on the PMU data quality can be performed. The common issues include data missing, bad data,

and data noises from communication channels. The sensitivity of the proposed methods to PMU data quality can also be investigated.

Appendix A

VOLTAGE STABILITY CRITERION PROOF

In this appendix, we prove that, for the system from Chapter 2, replotted here in Fig. A.1, when $Z_{ln} = Z_{ld}$, the maximum real power is transferred; and with a constant-power load characteristic, the system becomes unstable. Therefore, $Z_{ln} = Z_{ld}$ can be used as the criterion for voltage stability.

A.1 Maximum Power Transferred When $Z_{ln} = Z_{ld}$

Statement: Assuming the source and line impedance (i.e., $\bar{E}_s$ and $\bar{Z}_{ln}$) are constant and the load power factor is also fixed, the active power transferred to the load is maximum when $Z_{ln} = Z_{ld}$.

Proof: The fixed load power factor implies that the angle of the load impedance (i.e.,ϕ_{ld}) is also fixed. Therefore, the complex power transferred to load is

$$\bar{S} = \bar{V} \cdot \bar{I}^* = \bar{I}\bar{Z}_{ld} \cdot \bar{I}^* = I^2 \cdot \bar{Z}_{ld} = |\frac{\bar{E}_s}{\bar{Z}_{ln} + \bar{Z}_{ld}}|^2 \cdot \bar{Z}_{ld}. \tag{A.1}$$

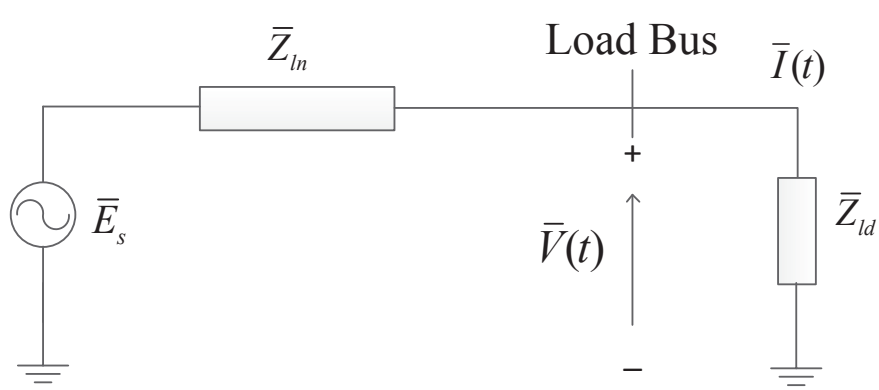

Figure A.1: Voltage stability illustration.

According to cosine formula,

$$|\bar{Z}_{ln} + \bar{Z}_{ld}|^2 = Z_{ln}^2 + Z_{ld}^2 - 2Z_{ln}Z_{ld}\cos(\phi_{ln} - \phi_{ld}). \tag{A.2}$$

Then

$$\bar{S} = \frac{E_s^2}{Z_{ln}^2 + Z_{ld}^2 - 2Z_{ln}Z_{ld}\cos(\phi_{ln} - \phi_{ld})}\bar{Z}_{ld}. \tag{A.3}$$

Then eventually,

$$P = Re\{\bar{S}\} = \frac{E_s^2}{Z_{ln}^2 + Z_{ld}^2 - 2Z_{ln}Z_{ld}\cos(\phi_{ln} - \phi_{ld})}Z_{ld}\cos(\phi_{ld}) \tag{A.4}$$

$$= \frac{E_s^2}{\frac{Z_{ln}^2}{Z_{ld}} + Z_{ld} - 2Z_{ln}\cos(\phi_{ln} - \phi_{ld})}\cos(\phi_{ld}). \tag{A.5}$$

In equation (A.5), since E_s, Z_{ln}, ϕ_{ln} and ϕ_{ld} are fixed, when $Z_{ld} = Z_{ln}$, the denominator reaches the minimum and sequentially, the active power reaches the maximum.

A.2 System Becomes Unstable When $Z_{ln} = Z_{ld}$

Statement: For the same system in Fig. A.1, the source $\bar{E}_s$ and line impedance $\bar{Z}_{ln}$ are constant. With constant-power load characteristics, when $Z_{ln} = Z_{ld}$, the system becomes unstable, which implies that the Q-V sensitivity becomes negative.

Proof: Without loss of generality, let $\bar{E}_s = 1\angle 0^o$ and $\frac{1}{\bar{Z}_{ln}} = \bar{Y}_{ln} = Y_{ln}\angle\beta_{ln}$.

The complex power can also be expressed as

$$\begin{aligned}\bar{S} &= \bar{V}\cdot\bar{I}^* = \bar{V}\cdot[(\bar{E}_s - \bar{Y})\bar{Y}_{ln}]^* \\ &= V\angle\theta[(1\angle 0^o - V\angle\theta)Y_{ln}\angle\beta_{ln}]^* \\ &= VY\angle(\theta - \beta_{ln}) - V^2Y\angle(-\beta_{ln}).\end{aligned} \tag{A.6}$$

The active power and reactive power can be easily expressed as

$$P = Re\{\bar{S}\} = VY\cos(\theta - \beta_{ln}) - V^2Y\cos(\beta_{ln}); \tag{A.7}$$

$$Q = Im\{\bar{S}\} = VY\sin(\theta - \beta_{ln}) + V^2Y\sin(\beta_{ln}). \tag{A.8}$$

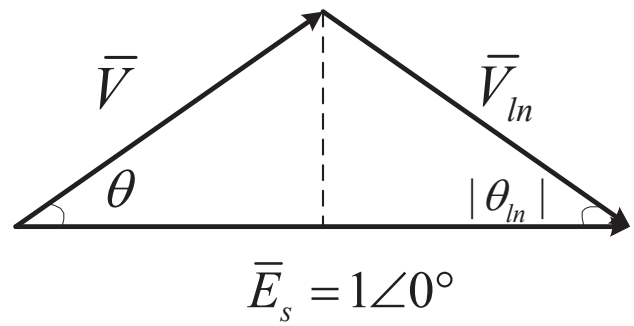

Figure A.2: Voltage vector diagram.

In this statement, with the constant load power characteristics, we assume that the load impedance, both magnitude and angle, can be varied to maintain constant active power. From equation (A.7), the variable θ can be expressed with P as

$$\theta = \cos^{-1} \frac{P + V^2 Y \cos(\beta_{ln})}{VY} + \beta_{ln}. \tag{A.9}$$

Substituting it into equation (A.8), we can get

$$Q = \sqrt{V^2Y^2 - (P + V^2 Y \cos(\beta_{ln}))^2} + V^2 Y \sin(\beta_{ln}). \tag{A.10}$$

Taking the derivative of Q with respect to V, we get

$$\frac{\partial Q}{\partial V} = \frac{VY^2 - 2VY(P + V^2 Y)\cos(\beta_{ln})}{\sqrt{V^2Y^2 - (P + V^2 Y \cos(\beta_{ln}))^2}} + 2VY \sin(\beta_{ln}). \tag{A.11}$$

To find the critical point of the voltage stability, set the derivative in (A.11) to be 0. Then we can calculate P out as

$$P = \frac{Y \cos(\beta_{ln})}{2} - V^2 Y \cos(\beta_{ln}) + VY \sin(\beta_{ln}) \sqrt{1 - \frac{1}{4V^2}}. \tag{A.12}$$

On the other side, when $Z_{ln} = Z_{ld}$, since $Z_{ln} \cdot I = Z_{ld} \cdot I$, the magnitude of the voltage drop across the transmission line, noted as $|\bar{V_{ln}}|$, should be equal to the load voltage magnitude V. Furthermore, as shown in Fig. A.2, since $\bar{V}_{ln} + \bar{V} = \bar{E} = 1\angle 0^o$, $\bar{V}_{ln}$ and $\bar{V}$ should be conjugate to each other and the cosine of θ, which is the angle of the load voltage can be determined by

$$\cos(\theta) = \frac{1}{2V}. \tag{A.13}$$

The complex power transferred into the load is

$$\begin{aligned}\bar{S} &= \bar{V} \cdot \bar{I}^* = \bar{V} \cdot [\bar{V}_{ls} \cdot \bar{Y}_{ln}]^* \\ &= V\angle\theta \cdot [V\angle(-\theta) \cdot Y_{ln}\angle(\beta_{ln})]^* = V^2 Y_{ln}\angle(2\theta - \beta_{ln}).\end{aligned} \tag{A.14}$$

With

$$\cos(2\theta) = 2\cos^2\theta - 1 = \frac{1}{2V^2} - 1; \tag{A.15}$$

$$\sin(2\theta) = 2\sin\theta\cos\theta = \frac{1}{V}\sqrt{1 - \frac{1}{4V^2}}, \tag{A.16}$$

the active power can be calculated out as

$$\begin{aligned}P = Re\{\bar{S}\} &= V^2 Y\cos(2\theta - \beta_{ln}) = V^2 Y[\cos(2\theta)\cos\beta_{ln} + \sin(2\theta)\sin(\beta_{ln})] \\ &= \frac{Y\cos(\beta_{ln})}{2} - V^2 Y\cos(\beta_{ln}) + VY\sqrt{1 - \frac{1}{4V^2}}\sin(\beta_{ln}),\end{aligned} \tag{A.17}$$

which is exactly the same with (A.12).

At this point, we can confidently say that with constant power load characteristics, $Z_{ln} = Z_{ld}$ is the critical point of voltage stability.

Appendix B

TWO-AREA TEST SYSTEM EXPERIMENT MEASUREMENTS

Table B.1: Bus information when system close to collapse

	bus #	V [p.u.]	θ[deg]	P [p.u.]	Q [p.u.]
t_1	1	1.0300	18.50	7.9190	2.0758
	2	1.0100	7.17	7.7000	2.4116
	3	0.9669	-9.66	0	0
	4	0.9596	-12.98	-10.7360	1.1000
	10	1.0046	11.16	0	0
	11	1.0300	-10.61	7.8760	2.1547
	12	1.0100	-21.86	7.7000	2.6279
	13	0.9604	-38.78	0	0
	14	0.9692	-44.64	-19.4150	-1.1000
	20	0.9784	-0.31	0	0
	101	0.9982	-24.57	0	0
	110	1.0032	-17.92	0	0
	120	0.9749	-29.37	0	0
t_2	1	1.0300	18.50	8.6055	2.8985
	2	1.0100	5.71	8.1900	3.9510
	3	0.9288	-13.09	0	0
	4	0.9596	-16.62	-11.4192	-1.1700
	10	0.9929	10.42	0	0
	11	1.0300	-17.06	8.3772	3.0349
	12	1.0100	-29.35	8.1900	4.4419
	13	0.9134	-48.30	0	0
	14	0.9597	-54.6532	-20.6505	-1.1700
	20	0.9543	-2.4507	0	0
	101	0.9396	-30.9457	0	0
	110	0.9902	-24.9412	0	0
	120	0.9463	-37.5737	0	0

Table B.2: Line value when system close to collapse

		t_1		t_2	
From Bus #	To Bus #	P [p.u.]	Q [p.u.]	P [p.u.]	Q [p.u.]
1	10	7.9190	2.0758	8.6055	2.8985
2	20	7.7000	2.4116	8.1900	3.9510
3	4	10.7360	1.7324	11.4192	1.8855
3	20	-15.2106	1.6586	-16.2926	0.7743
3	101	2.2373	-0.2930	2.4367	-0.0360
3	101	2.2373	-0.2930	2.4367	-0.0360
10	20	7.9190	1.0208	8.6055	1.6005
11	110	7.8760	2.1547	8.3772	3.0349
12	120	7.7000	2.6279	8.1900	4.4419
13	101	-2.1239	0.0604	-2.2901	0.2864
13	101	-2.1239	0.0604	-2.2901	0.2864
13	14	19.4150	3.1127	20.6505	3.4927
13	120	-15.1673	1.3786	-16.0704	0.1061
110	120	7.8760	1.1052	8.3772	1.7852

Table B.3: Two sets of PMU measurements when the system close to collapse

	t_1	t_2
V_1 [p.u.]	0.9669	0.9288
θ_1 [deg]	-9.66	-13.09
I_1 [p.u.]	2.3335	2.6238
γ_1 [deg]	-2.1996	-12.2488
V_2 [p.u.]	0.9604	0.9134
θ_2 [deg]	-38.78	-48.30
I_2 [p.u.]	2.2123	2.5267
γ_2 [deg]	142.8520	138.8328

Appendix C

RTDS TESTBED SYSTEM

For Example 1 in Chapter 5, the voltage and current phasors FFT analysis results are presented in Fig. C.1 and C.2 respectively, from which it is verified again that the dominant frequency stays constant for all the observables.

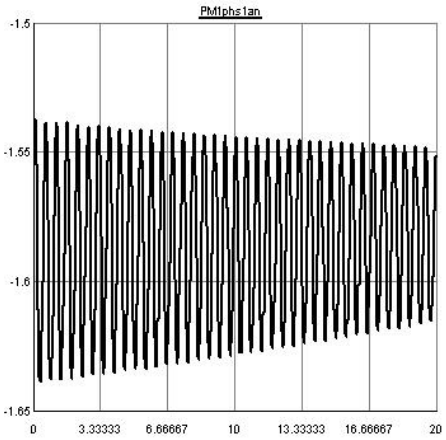

(a) The angle of voltage phasor along with time.

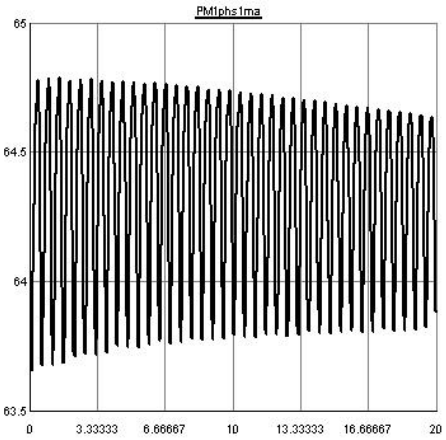

(b) The magnitude of voltage phasor along with time.

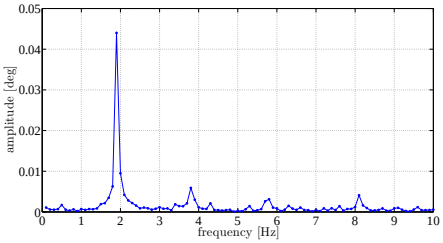

(c) Frequency spectra of voltage angle.

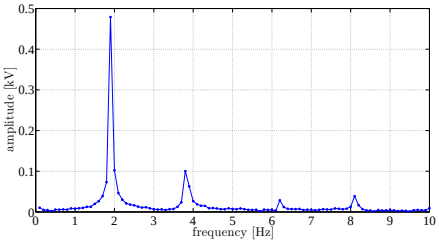

(d) Frequency spectra of voltage magnitude.

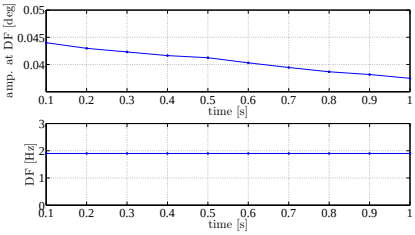

(e) Dominant frequency of voltage angle and its magnitude along wiht time.

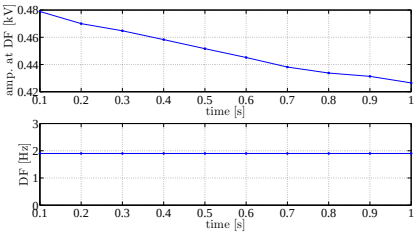

(f) Dominant frequency of voltage magnitude and its magnitude along wiht time.

Figure C.1: Voltage phasor FFT analysis.

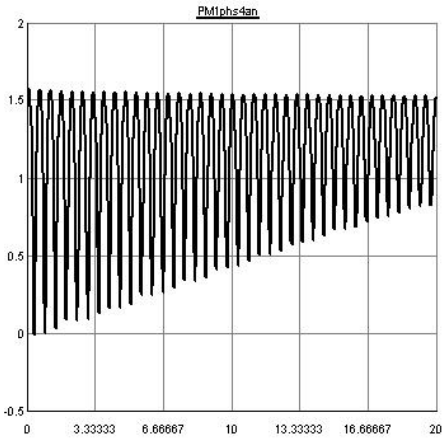

(a) The angle of current phasor along with time.

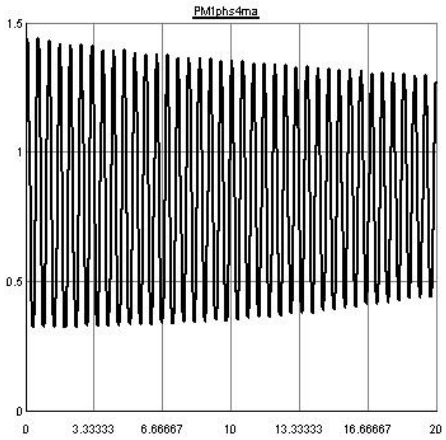

(b) The magnitude of current phasor along with time.

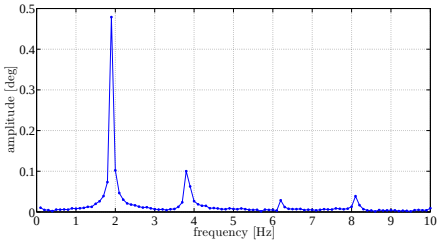

(c) Frequency spectra of current angle.

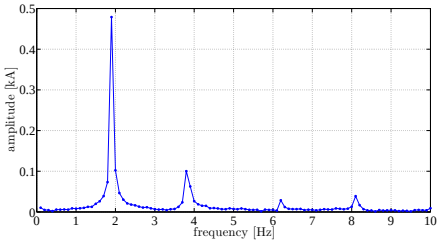

(d) Frequency spectra of current magnitude.

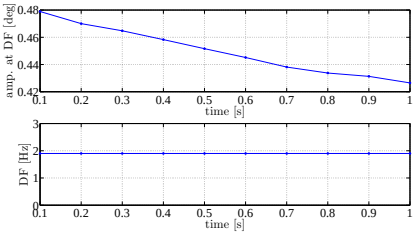

(e) Dominant frequency of current angle and its magnitude along wiht time.

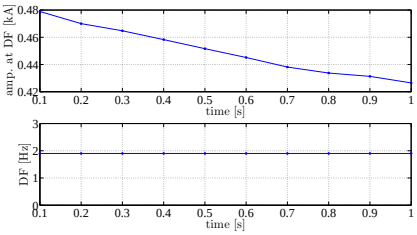

(f) Dominant frequency of current magnitude and its magnitude along wiht time.

Figure C.2: Current phasor FFT analysis.

REFERENCES

[1] P. Kundur, *Power System Stability and Control*. New York: McGraw-Hill, 1994.

[2] A. Phadke and J. Thorp, *Synchronized Phasor Measurements and Their Applications*. New York: Springer, 2008.

[3] G. Liu, J. Quintero, and V. Venkatasubramanian, "Oscillation monitoring system based on wide area synchrophasors in power systems," in *Bulk Power System Dynamics and Control - VII. Revitalizing Operational Reliability, 2007 iREP Symposium*, Aug. 2007, pp. 1 –13.

[4] D. Ruiz-Vega, A. Messina, and M. Pavella, "Online assessment and control of transient oscillations damping," *Power Systems, IEEE Transactions on*, vol. 19, no. 2, pp. 1038 – 1047, May 2004.

[5] Z. Yuan, T. Xia, Y. Zhang, L. Chen, P. Markham, R. Gardner, and Y. Liu, "Inter-area oscillation analysis using wide area voltage angle measurements from fnet," in *Power and Energy Society General Meeting, 2010 IEEE*, Jul. 2010, pp. 1 –7.

[6] K. Vu, M. Begovic, D. Novosel, and M. Saha, "Use of local measurements to estimate voltage-stability margin," *Power Systems, IEEE Transactions on*, vol. 14, no. 3, pp. 1029 –1035, Aug. 1999.

[7] S. Corsi, "Wide area voltage protection," *Generation, Transmission Distribution, IET*, vol. 4, no. 10, pp. 1164 –1179, Oct. 2010.

[8] J. Chow, A. Chakrabortty, L. Vanfretti, and M. Arcak, "Estimation of radial power system transfer path dynamic parameters using synchronized phasor data," *Power Systems, IEEE Transactions on*, vol. 23, no. 2, pp. 564 –571, May 2008.

[9] A. Chakrabortty, J. Chow, and A. Salazar, "A measurement-based framework for dynamic equivalencing of large power systems using WAMS," in *Innovative Smart Grid Technologies (ISGT), 2010*, Jan. 2010, pp. 1 –8.

[10] R. Gutman, "Application of line loadability concepts to operating studies," *Power Systems, IEEE Transactions on*, vol. 3, no. 4, pp. 1426 –1433, Nov. 1988.

[11] U.S. Department of Energy, "Smart grid investment grant program: progress report," Tech. Rep., Jul. 2012.

[12] B. Milosevic and M. Begovic, "Voltage-stability protection and control using a wide-area network of phasor measurements," *Power Systems, IEEE Transactions on*, vol. 18, no. 1, pp. 121 – 127, Feb. 2003.

[13] S. Abdelkader and D. Morrow, "Online tracking of thevenin equivalent parameters using pmu measurements," *Power Systems, IEEE Transactions on*, vol. 27, no. 2, pp. 975 –983, May 2012.

[14] L. Ljung, *System Identification: Theory for the User.* Upper Saddle Rever, NJ: Prentice-Hall, Inc., 1999.

[15] Y. Song, "Design of secondary voltage and stability controls with multiple control objectives," Ph.D. dissertation, Georgia Institute of Technology, Dec. 2008.

[16] D. Kosterev, C. Taylor, and W. Mittelstadt, "Model validation for the August 10, 1996 WSCC system outage," *Power Systems, IEEE Transactions on*, vol. 14, no. 3, pp. 967 –979, Aug. 1999.

[17] P. Sauer and M. Pai, *Power System Dynamics and Stability.* Upper Saddle Rever, NJ: Prentice-Hall, Inc., 1998.

[18] J. Zhang and D. Chen, "On the application of phasor measurement units to power system stability monitoring and analysis," in *Power and Energy Conference at Illinois (PECI), 2012 IEEE*, Feb. 2012, pp. 1 –6.

[19] J. Glover, M. Sama, and T. Overbye, *Power Systems Analysis and Design.* Upper Saddle Rever, NJ: Thompson-Engineering, 2008.

[20] H. P. S. Clair, "Practical concepts in capability and performance of transmission lines," *Power Apparatus and Systems, Part III. Transactions of the American Institute of Electrical Engineers*, vol. 72, no. 2, pp. 1152 –1157, Jan. 1953.

[21] R. Gutman, P. Marchenko, and R. Dunlop, "Analytical development of loadability characteristics for EHV and UHV transmission lines," *Power Apparatus and Systems, IEEE Transactions on*, vol. PAS-98, no. 2, pp. 606 –617, Mar. 1979.

[22] L. O. Chua and P.-M. Lin, *Computer-Aided Analysis of Electronic Circuits.* Upper Saddle Rever, NJ: Prentice-Hall, Inc., 1975.

[23] A. Meliopoulos, G. Cokkinides, O. Wasynczuk, E. Coyle, M. Bell, C. Hoffmann, C. Nita-Rotaru, T. Downar, L. Tsoukalas, and R. Gao, "PMU data characterization and application to stability monitoring," in *Power Systems Conference and Exposition, 2006.*, Nov. 2006, pp. 151 –158.

[24] Q. Liu, "Oscillation monitoring system based on wide area phasor measurements in power systems," Ph.D. dissertation, Washington State University, Aug. 2010.

[25] A. V. Oppenheim, A. S. Willsky, and S. Hamid, *Signal and Systems.* Upper Saddle Rever, NJ: Prentice-Hall, Inc., 1996.

[26] S. Salivahanan and A. Vallavaraj, *Digital Signal Processing.* New York: McGraw-Hill Education, 2001.

[27] "IEEE recommended practice for excitation system models for power system stability studies," *IEEE Std 421.5-2005 (revision of IEEE Std 421.5-1992)*, pp. 1 –85, 2006.

[28] "IEEE recommended practice for functional and performance characteristics of control systems for steam turbine-generator units," *IEEE Std 122-1991*, p. 1, 1992.

[29] RTDS Technologies Inc., "RSCAD software suite." [Online]. Available: http://www.rtds.com/software/rscad/rscad.html

[30] Schweitzer Engineering Laboratories, "SEL-421-4,-5 protection, automation, and control system." [Online]. Available: https://www.selinc.com/SEL-421/